DTU Library

Diffusion and sorption of organic micropollutants in biofilms with varying thicknesses

Torresi, Elena; Polesel, Fabio; Bester, Kai; Christensson, Magnus; Smets, Barth F.; Trapp, Stefan; Andersen, Henrik Rasmus; Plósz, Benedek G.

1

2

3

Diffusion and sorption of organic micropollutants in biofilms with varying thicknesses

6

7 Elena Torresi[1,2†**], Fabio Polesel[1†], Kai Bester[3], Magnus Christensson[2], Barth F. Smets[1],

8 Stefan Trapp[1], Henrik R. Andersen[1], Benedek Gy. Plósz[1,4]*

9

10 [1]DTU Environment, Technical University of Denmark, Bygningstorvet B115, 2800 Kongens Lyngby, Denmark

11 [2]Veolia Water Technologies AB, AnoxKaldnes, Klosterängsvägen 11A, SE-226 47 Lund, Sweden

12 [3]Department of Environmental Science, Århus University, Frederiksborgvej 399, 4000 Roskilde, Denmark

13 [4]Department of Chemical Engineering, University of Bath, Claverton Down, Bath BA2 7AY, UK

14

15

16 † Joint first authors.

17

18

19 *Benedek Gy. Plósz: b.g.plosz@bath.ac.uk

20 **Elena Torresi: elto@env.dtu.dk

21

22
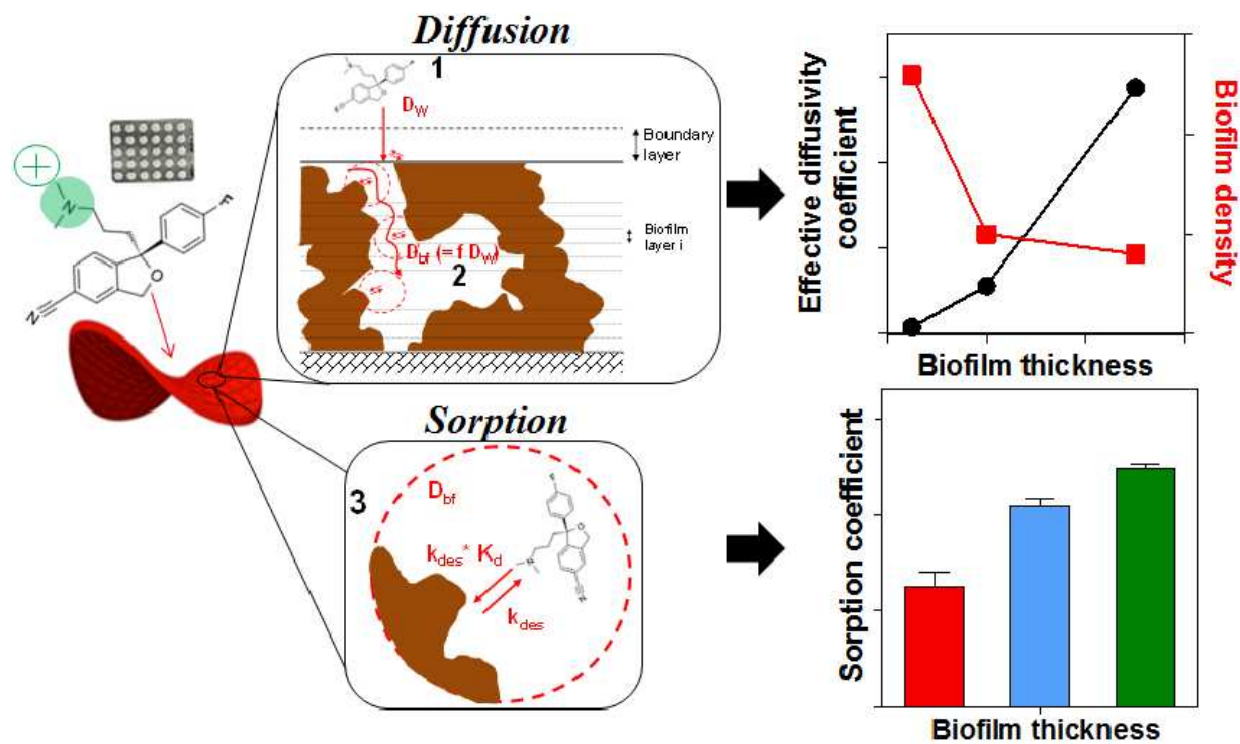
23 **Abstract**

24 Solid-liquid partitioning is one of the main fate processes determining the removal of

25 micropollutants in wastewater. Little is known on the sorption of micropollutants in biofilms,

26 where molecular diffusion may significantly influence partitioning kinetics. In this study, the

27 diffusion and the sorption of 23 micropollutants were investigated in novel moving bed biofilm

28 reactor (MBBR) carriers with controlled biofilm thickness (50, 200 and 500 µm) using targeted

29 batch experiments (initial concentration=1 µg L^{-1}, for X-ray contrast media 15 µg L^{-1}) and

30 mathematical modelling. We assessed the influence of biofilm thickness and density on the

31 dimensionless effective diffusivity coefficient f (-, equal to the biofilm-to-aqueous diffusivity

32 ratio) and the distribution coefficient $K_{d,eq}$ (L g^{-1}). Sorption was significant only for eight

33 positively charged micropollutants (atenolol, metoprolol, propranolol, citalopram, venlafaxine,

34 erythromycin, clarithromycin and roxithromycin), revealing the importance of electrostatic

35 interactions with solids. Sorption equilibria were likely not reached within the duration of

36 batch experiments (4 h), particularly for the thickest biofilm, requiring the calculation of the

37 distribution coefficient $K_{d,eq}$ based on the approximation of the asymptotic equilibrium

38 concentration (t > 4 h). $K_{d,eq}$ values increased with increasing biofilm thickness for all sorptive

39 micropollutants (except atenolol), possibly due to higher porosity and accessible surface area

40 in the thickest biofilm. Positive correlations between $K_{d,eq}$ and micropollutant properties

41 (polarity and molecular size descriptors) were identified but not for all biofilm thicknesses,

42 thus confirming the challenge of improving predictive sorption models for positively charged

43 compounds. A diffusion-sorption model was developed and calibrated against experimental

44 data, and estimated f values also increased with increasing biofilm thickness. This indicates

45 that diffusion in thinner biofilms may be strongly limited ($f \ll 0.1$) by the higher biomass

46 density (lower porosity) compared to thicker biofilms.

47

48 **Keywords:** Pharmaceuticals, wastewater, moving bed biofilm reactor, partitioning, biofilm

49 density, ionizable chemicals

50

1. Introduction

In wastewater treatment systems, partitioning of organic micropollutants to solid matrices is one of the mechanisms leading to their removal from the aqueous phase. The extent of partitioning is typically compound-dependent, and is governed by its affinity for organic phase (i.e., hydrophobic partitioning) and/or by electrostatic and other similar interactions between ionized molecules and charged solid surfaces (i.e., non-hydrophobic partitioning) (Franco and Trapp, 2008; Hyland et al., 2012; Ternes et al., 2004; Mackay and Vasudevan, 2012; Polesel et al., 2015).

Partitioning describes the distribution of molecules between the aqueous and the solid phase. At equilibrium, sorption and desorption rates are equal, and the ratio of sorbed and dissolved concentrations—normalized to the concentration of solids—is defined as the (linear) solid-liquid partition coefficient K_d (expressed in units of L kg^{-1} or, alternatively, L g^{-1}) (Joss et al., 2006; Ternes et al., 2004). Non-linear expressions (Freundlich and Langmuir isotherms) have been also used to describe partitioning equilibria to account for saturation of solid surfaces or synergistic effects (Delle Site, 2001).

Solid-liquid partitioning has been characterized for activated sludge biomass for a high number of pharmaceuticals Considerably less evidence is available for wastewater treatment biofilms, being limited to antibiotics (sulfamethoxazole, erythromycin, ciprofloxacin, tetracycline) and psycho-active drugs (fluoxetine) in biofilters (Wunder et al., 2011) and granules (Alvarino et al., 2015; Shi et al., 2011). Additionally, partitioning kinetics of other organic contaminants (polycyclic aromatic hydrocarbons, estrogens, nonylphenols, biocides) have been assessed for pure culture biofilms (Wicke et al., 2008, 2007) and river biofilms (Headley et al., 1998; Writer et al., 2011).

Although considered a fast process, partitioning is influenced by mass transfer limitation through diffusive boundary layers and inside the solid matrices, which likely determines the

75 time needed to achieve equilibrium between aqueous and sorbed concentrations (Joss et al.,

76 2004, 2006). While for activated sludge the equilibrium time is sufficiently fast to prevent an

77 empirical evaluation of mass transfer limitation (Joss et al., 2004; Plósz et al., 2010; Barret et

78 al., 2011), molecular diffusion may have a major role in determining partitioning kinetics in

79 biofilms. Biofilm characteristics such as biomass density and porosity have been found to

80 influence intra-biofilm diffusion of a number of organic and inorganic chemical compounds.

81 This effect has been described by introducing a coefficient f, defined as the ratio of effective

82 diffusivity in biofilms and in free aqueous media, thus defining diffusivity reduction in

83 biofilms (Fan et al., 1990; Guimerà et al., 2016; Horn and Morgenroth, 2006; Trapp and

84 Matthies, 1998; Zhang and Bishop, 1994a). While f was determined for a number of organic and

85 inorganic chemical compounds, no conclusive evidence currently exists for organic micropollutant

86 diffusion in biofilms, which was therefore investigated in this study.

87 In our previous work (Torresi et al., 2016), we investigated the biological transformation of

88 pharmaceuticals in nitrifying moving bed biofilm reactors (MBBRs) using novel MBBR

89 carriers (AnoxKaldnes Z-carriers), allowing the control of the biofilm thickness.

90 In this study, the main objective set was to assess how the diffusion and partitioning of 23

91 selected pharmaceuticals vary at different biofilm thicknesses (50, 200 and 500 µm) and to

92 quantify corresponding single point K_d values at environmentally relevant concentration levels.

93 By developing and calibrating a model that describes diffusive transport and partitioning in

94 biofilms, we aimed at elucidating the influence of biofilm thickness on (i) the molecular

95 diffusion of micropollutants within biofilm matrix, described by the dimensionless effective

96 diffusivity coefficient f; (ii) the extent of partitioning, described by coefficient K_d.

97 Additionally, using experimental and modelling results, the influence of biofilm characteristics

98 (porosity, density) and molecular properties (e.g., hydrophobicity, ionization) on the mass

99   transfer limitation and sorption of micropollutants in biofilms were assessed.

100 **2. Model development**

101

102 *2.1 Conceptual approach for diffusion and sorption in biofilms and model implementation*

103 Considering molecular diffusion of dissolved micropollutants from the bulk aqueous phase into

104 biofilms as the dominant mechanism (Zhang and Bishop, 1994a), the partitioning of organic

105 micropollutants consists of three consecutive steps (Joss et al., 2004): (1) diffusion of

106 dissolved micropollutant from bulk aqueous phase, through a boundary layer, into the biofilm

107 matrix; (2) diffusion of dissolved micropollutant through the biofilm matrix via its pores; (3)

108 sorption to the solid phase of the biofilm matrix (Fig. 1a). The diffusivity of organic chemicals

109 in a free aqueous medium ($D_{W,i}$, m^2 d^{-1}) can be predicted from properties of the chemical (e.g.,

110 molar volume) and of the medium. In this study, $D_{W,i}$ values for each chemical were calculated

111 according to Hayduk and Laudie (1974), although alternative approaches were also tested

112 (Table S1 in Supplementary Information).

113 Transport from the bulk liquid to the biofilm is controlled by the diffusion through a boundary

114 layer, for which the diffusivity was assumed equal to $D_{W,i}$ (**Assumption I**, Fig 1b). The

115 thickness of the boundary layer, L_L (µm), was assumed to be equal to 10 µm for all the Z-

116 carriers (Brockmann et al., 2008, see section 1 in SI). In biofilms, molecular diffusivity is

117 reduced compared to free aqueous media (Wanner and Reichert, 1996). This has been

118 attributed to the "tortuosity" of the transport path in biofilms, i.e. the increased (non-linear)

119 path length needed for diffusive transport as compared to free aqueous media (Zhang and

120 Bishop, 1994b). Molecular diffusivity reduction is described by the dimensionless coefficient

121 *f*, resulting in Eq. 1:

122 $D_{bf,i} = f \cdot D_{W,i}$ (Eq. 1)

7

123   where $D_{bf,i}$ (m^2 d^{-1}) is the effective diffusivity of micropollutants within biofilms and f (-) is

124   always lower than 1. While f values of 0.5–0.8 have been assigned for micropollutant diffusion

125   (Ort and Gujer, 2008; Vasiliadou et al., 2014), this parameter is likely to vary significantly

126   depending on the biofilm structure and properties (biofilm thickness, density, porosity and

127   tortuosity).

128   It has previously been shown that biofilm porosity and density can vary over the biofilm depth

129   (Zhang and Bishop, 1994a). In the model, we assume the biofilm as a homogenous porous

130   medium (**Assumption II**), although we accept that biofilms with different depth can have

131   different average porosities and densities. As a consequence, only one f value was used to

132   describe diffusion reduction into a biofilm with a certain thickness.

133   Sorption/desorption kinetics were described using first-order rate equations (see matrix in Fig.

134   1c). Sorption was considered as an equilibrium process (**Assumption III**), by attributing an

135   arbitrarily high value to the desorption rate k_{des}, thereby making diffusion from the bulk

136   aqueous phase and within the biofilm the rate-limiting steps for solid-liquid partitioning. At

137   micropollutant concentration levels targeted in this study (ng L^{-1} to µg L^{-1}), sorption can be

138   considered linear and better described by the distribution coefficient K_d (**Assumption IV**).

139   Based on the presented conceptual approach, a diffusion-sorption model was implemented as

140   one-dimensional biofilm model in Aquasim 2.1 (Reichert, 1994). Design and measured biofilm

141   properties (biofilm thickness, surface area, biomass density, porosity) were used as input to the

142   model (see Table 1). Each biofilm was spatially discretized in 20 completely mixed layers.

143   This allowed solving the generic mass balance equation for dissolved micropollutant

144   concentration C_L (ng L^{-1}) in biofilm (Eq. 2):

145    $$\frac{\partial C_L}{\partial t} = D_{bf,i}\frac{\partial^2 C_L}{\partial z^2} - k_{des}K_d C_L X + k_{des}C_S \qquad\text{(Eq. 2)}$$

146 (where X is the biomass concentration in biofilm, g L^{-1}; C_S is the sorbed micropollutant

147 concentration, ng L^{-1}; C_L varies with time t and depth z) as a set of ordinary differential

148 equations by using the method of lines (Wanner and Reichert, 1996). According to the

149 diffusion-sorption model, micropollutants undergo equilibrium microscale partitioning as they

150 diffuse through biofilm, in analogy to the approach proposed by Wu and Gschwend (1986).

151 Further details on the conceptual biofilm model, on microscopic mass balances and on the

152 initial conditions are given in the Supplementary Information (section S1 and Figure S1).

153 **< Figure 1 >**

154

155 *2.2 Calculation of sorption coefficients*

156 At equilibrium, the micropollutant concentration sorbed onto biomass ($C_{S,eq}$, µg L^{-1}) is

157 proportional to the dissolved concentration ($C_{L,eq}$, µg L^{-1}), and their ratio, normalized by the

158 concentration of solids ($X_{biomass}$, g L^{-1}), is used to calculate the sorption coefficient $K_{d,eq}$ (L g^{-1}).

159 With negligible transformation, it is commonly assumed (e.g., in activated sludge) that the

160 sorbed concentration is equivalent to the decrease in dissolved concentration ($C_{L,0} - C_{L,eq}$)

161 between the beginning and the end of batch sorption experiments.

162 When considering biofilm systems, transport in biofilm pores, along with sorption, can also

163 determine a decrease of micropollutant concentrations in the bulk phase. Hence, the coefficient

164 $K_{d,eq}$ (L g^{-1}) was defined to describe sorption in Z-carrier biofilms based on mass balance

165 considerations (Eq. 3):

166
$$K_{d,eq} = \frac{\left[\dfrac{C_{L,0} V_{bulk}}{V_{bulk} + V_{bf,wet}} - \dfrac{C_{L,eq}(V_{bulk} + V_{PW})}{V_{bulk} + V_{bf,wet}} \right]}{C_{L,eq} X_{biomass}}$$
(Eq. 3)

167 where V_{bulk} (L) denotes the volume of the bulk liquid, $V_{bf,wet}$ (L) the volume of wet biofilm

168 (equal to the total surface area of Z-carriers times the defined biofilm thickness) and V_{PW} (L)

9

169   the volume of the pore water in the biofilm matrix, not accounting for cellular water content

170   (see 3.4). The procedure used to derive Eq. 3 is presented in detail in the Supplementary

171   Information (section S3).

172   The 'asymptotic' concentration $C_{L,eq}$, defining true sorption equilibrium, was estimated by

173   fitting measured concentration profiles in batch sorption experiments with a first-order decay

174   equation (Eq. 4)

175    $$C_L(t) = (C_{L,0} - C_{L,eq})e^{-kt} + C_{L,eq}$$ (Eq. 4)

176   In activated sludge, it has been widely accepted that sorption equilibrium can be reached

177   within 0.5–1 h (Ternes et al., 2004; Andersen et al., 2005; Yi and Harper, 2007, Hörsing et al.,

178   2011). To verify whether sorption equilibrium was achieved relatively fast (i.e., within the 4-

179   hour duration of sorption experiments) also in Z-carrier biofilms, the sorption coefficient $K_{d,4h}$

180   (L g^{-1}) was calculated (Eq. 5):

181    $$K_{d,4h} = \frac{\left[\dfrac{C_{L,0}V_{bulk}}{V_{bulk}+V_{bf,wet}} - \dfrac{C_{L,4h}(V_{bulk}+V_{PW})}{V_{bulk}+V_{bf,wet}}\right]}{C_{L,4h}X_{biomass}}$$ (Eq. 5)

182   where $C_{L,4h}$ is the measured dissolved concentration in bulk aqueous phase at t=4 h (the last

183   measurement in sorption experiments), replacing $C_{L,eq}$ in Eq. 3. Specifically, the 4-hour

184   equilibrium assumption was verified by comparing $K_{d,4h}$ and $K_{d,eq}$ and assessing the relative

185   deviation between the two coefficients.

186   As mentioned above, the decrease of bulk micropollutant concentration during sorption

187   experiments with biofilms results from transport in biofilm pores (besides sorption in

188   biofilms). To verify the impact of neglecting mass transfer to biofilm pores on sorption

189   coefficient determination, the sorption coefficient $K_{d,susp}$ was calculated (Eq. 6):

190    $$K_{d,susp} = \frac{C_{L,0} - C_{L,eq}}{C_{L,eq}X_{biomass}}$$ (Eq. 6)

191   where $C_{L,eq}$ was calculated using Eq. 4. Notably, Eq. 6 is commonly used to describe sorption

192   onto suspended activated sludge, where the effect of porosity is neglected. The comparison

193   between $K_{d,eq}$ and $K_{d,susp}$ (together with relative deviation the two coefficients) was used to

194   quantify the contribution of transport to biofilm pores, hence the impact of porosity, on the

195   estimated sorption coefficient.

196

197   *2.3 Parameter estimation approach*

198   The assessment of diffusion and sorption of micropollutants in biofilms consisted of two main

199   consecutive steps performed for each micropollutant and at different biofilm thicknesses: (i)

200   calculation of the coefficient $K_{d,eq}$ (section 2.2); (ii) calibration of the diffusion-sorption model

201   (section 2.1) against experimental data and estimation of the coefficient *f*, which was the only

202   parameters fitted in the model. Estimation of *f* was performed using the secant model

203   calibration algorithm embedded in Aquasim 2.1.

3. Materials and methods

3.1. System description and operation

Nitrifying MBBRs used in this study have been described elsewhere (Torresi et al., 2016). Briefly, two laboratory-scale nitrifying MBBRs were operated in parallel under continuous-flow conditions for approximately 300 days. Z-carriers (AnoxKaldnes AB, Lund, Sweden) were used to obtain biofilm of different thicknesses. Z-carriers have a saddle shaped grid covered surface allowing for biofilm growth only up to the height of the grid wall (Torresi et al., 2016). Three different Z-carriers (named Z50, Z200, and Z500) were used in this study, with the numbers indicating the grid wall height in µm (hence the maximum controlled biofilm thickness). Biofilms were enriched by feeding the MBBRs with effluent wastewater from a local municipal treatment plant (Källby, Lund, Sweden), spiked with ammonium (50 mg L^{-1} of NH_4-N as NH_4Cl) and phosphate (0.5 mg L^{-1} of PO_4-P as KH_2PO_4). The MBBRs were operated under similar conditions, i.e. hydraulic residence time of 2 h, dissolved oxygen concentration of 4.5 ± 0.5 mg L^{-1}, pH of 7.5 ± 0.5 and temperature of $20^{\circ}C$ (achieved using a thermostat).

3.2. Sorption batch experiments

Sorption batch experiments were performed after reaching stable nitrogen removal (Torresi et al., 2016), roughly, around day 300. Prior to batch experiments, the two MBBRs were disconnected and three types of Z-carriers (Z50, Z200, Z500) were manually separated. Subsequently, Z-carriers were left overnight at $4^{\circ}C$ in a beaker with tap water to allow for desorption of micropollutants possibly sorbed during continuous-flow operation.

Sorption batch experiments were carried out in three 200-mL glass beakers using filtered (0.2 µm Munktell MG/A glass fiber filters) effluent wastewater from Källby treatment plant. Ammonium and nitrate in the feed were at concentration of <0.5 mgN L^{-1} and 6 mgN L^{-1},

228 respectively, while organic carbon concentration was lower than 35 mgCOD L^{-1}, mostly in

229 inert form.

230 The biomass concentration in the three glass beakers was adjusted to 0.8 g L^{-1} based on

231 attached biomass concentration measurements for the different carriers and adjusting the

232 number of carriers accordingly (56 carriers for Z50, 32 for Z200 and 16 for Z500), resulting in

233 a total biofilm surface area of 0.06, 0.04, 0.02 m^2 for the batch containing Z50, Z200 and Z500

234 carriers, respectively. Other abiotic removal processes, such as volatilization, sorption of

235 micropollutants on plastic carriers and glass wall, had been previously assessed and found

236 negligible in MBBRs (Torresi et al., 2016).

237 Twenty-three micropollutants were spiked in all the beakers with an initial concentration of 1

238 µg L^{-1} except for X-ray contrast media (15 µg L^{-1}), as they are usually found at higher

239 concentrations in effluent wastewater (Margot et al., 2015). A stock solution, containing

240 micropollutants dissolved in methanol (40 mg L^{-1}), was first spiked into empty glass beakers

241 and the methanol was allowed to evaporate in the fumehood for approximately 1 hour.

242 Subsequently, the solution was resuspended in filtered effluent for approximately 30 min to

243 dissolve the spiked micropollutants. Biomass inactivation was achieved by: (i) addition of

244 allylthiourea (ATU, 10 mg L^{-1}, Tran et al., 2009; Khunjar and Love, 2011) and nitrogen

245 sparging (Hamon et al., 2014) to inhibit nitrfyng bacteria; and (ii) addition of sodium azide

246 (0.5 g L^{-1}; Rattier et al., 2014) to inhibit the activity of heterotrophic bacteria.

247 The experiment duration was set to 4 hours. Homogenous aqueous samples were collected at

248 regular intervals from the bulk phase in each beaker at 0, 5, 10, 30, 90 and 240 min. The batch

249 experiments were performed at ambient temperature and initial pH was measured to be 7.5 $\pm$

250 0.5. Since only one spiking concentration was tested, results from sorption experiments were

251 used to determine single point K_d values.

13

252

3.3. Chemicals

254 Twenty-three environmentally relevant micropollutants were selected for this study. The

255 targeted pharmaceuticals were grouped in six categories according to their use: (i) four beta-

256 blocker pharmaceuticals (atenolol, metoprolol, propranolol and sotalol); (ii) five X-ray contrast

257 media (diatrizoic acid, iohexol, iopamidol, iopromide, iomeprol); (iii) three sulfonamide

258 antibiotics (sulfadiazine, sulfamethizole and sulfamethoxazole), one metabolite (acetyl-

259 sulfadiazine) and one combination product (trimethoprim); (iv) three non-steroidal anti-

260 inflammatory pharmaceuticals (phenazone, diclofenac, ibuprofen); (v) three psycho-active

261 drugs (carbamazepine, venlafaxine and citalopram); (vi) three macrolide antibiotics

262 (erythromycin, clarithromycin and roxithromycin). Further information regarding chemical

263 structure and properties, CAS numbers and chemical suppliers can be found in Table S2–S3

264 and in Escolà Casas et al. (2015).

265

3.4. Analytical methods

267 Samples for micropollutant analysis were collected (4 mL) and analysed via direct injection

268 using internal standards (injected volume of 100 µL). Details regarding sample preparation,

269 internal standards, HPLC and mass spectrometry conditions, limits of detection and

270 quantification are shown in Escolà Casas et al. (2015). Biomass concentration on Z-carriers was

271 measured in two ways: (i) as attached biomass concentration (expressed as total attached

272 solids, TAS), calculated from the difference in weight of three dried carriers (105°C for > 24 h)

273 before and after biofilm removal (using 2M H_2SO_4 with subsequent brushing) (see also Escolà

274 Casas et al., 2015; Falås et al., 2013; Torresi et al., 2016); and (ii) by scraping and suspending

275 the biofilm in tap water and measuring total suspended solids (TSS) and volatile suspended

276 solids (VSS) according to APHA standard methods (Clesceri, 1989). Biofilm properties such

277 as biofilm dry density ρ_d (g cm^{-3}), biomass density in wet biofilm ρ (kg m^{-3}) and porosity ε (%)

278 were calculated according to Tchobanoglous et al. (2003) and Hu et al. (2013) using measured

279 biofilm properties (e.g., solids content), as detailed in the Supplementary Information (section

280 S2). Porosity is defined as the fraction of the biofilm volume occupied only by water outside

281 the cells and not inside the cells (Hu et al., 2013). Furthermore, ρ_d denotes the dry mass of

282 biofilm per volume of dry biofilm (i.e., defines a *true* density) while ρ denotes the dry mass of

283 biomass per volume of wet biofilm (i.e., defines a concentration of biomass within the

284 biofilm). Further discussion on the calculation methodology used and on the biofilm properties

285 can be found in section S2.

286

287 *3.5. Statistical analysis and influence of chemical properties*

288 Pearson's and Spearman's correlations between $K_{d,eq}$ and chemical properties (expressed in

289 logarithmic base) were assessed at different biofilm thicknesses. A significance level of 0.05

290 was used for all statistical tests in this study. The investigated physico-chemical properties

291 include: the molecular volume MV (cm^3 mol^{-1}); the dissociation constant(s) pK_a; the number of

292 rotable bonds (nRB); the van der Waals area ($vdWA$, m^2 kmol^{-1}) (Sathyamoorthy and

293 Ramsburg, 2013); McGowan's approximation of the molecular volume (V_X, cm^3 mol^{-1}) (Droge

294 and Goss, 2013a); and the topological polar surface area (*TPSA,* Å^2) (Ertl et al., 2000).

295 Chemical properties and $K_{d,eq}$ were log transformed (Vasudevan et al., 2009) with exception of

296 nRB (Sathyamoorthy and Ramsburg, 2013) and molecular size descriptors MV and V_X.

297 Chemical properties for each compound were retrieved using ACD/Labs predictions and the

298 database Mol-inisticts (for log$vdWA$) or calculated based on previously defined equations (for

299 V_X: Abraham and McGowan, 1987; Droge and Goss, 2013a). Pearson's and Spearman's

300 correlations and their significance were assessed using GraphPad Prism 5.0. Furthermore,

301 possible correlations between f and the abovementioned properties were also investigated.

302 Significant differences between estimated f values for each chemical at different biofilm thickness

303 were determined by examining the overlap between standard deviations of the estimate (Cumming

304 et al., 2007)

4. Results and discussion

4.1. Biofilm properties

Measured and calculated values for a number of biofilm properties are reported in Table 1. Dry biofilm mass per surface area of carrier (gTAS m^{-2}, Table 1) increased with biofilm thickness, being approximately four times higher in Z500 compared to Z50. Biofilm thickness in Z-carriers was recently measured using optical coherence tomography (OCT), revealing good agreement between measured and nominal thickness based on carrier design (Piculell et al., 2016). Conversely, biofilm density in wet biofilm ρ (section 1 in SI) in Z50 was up to 3-fold higher as compared to Z200 and Z500. This suggests a change in biofilm porosity as a function of biofilm thickness. Biofilm porosity ε (Eq. S12), ranged from 75% (Z50) to 93% (Z500) (Table 1). An approximate porosity of 80% is commonly assumed in one-dimensional biofilm models (Wanner and Reichert, 1996; Brockmann et al., 2008) and similar values have been previously determined using modelling approximations (Zacarias et al., 2005; Zhang and Bishop, 1994b). The observed increasing ε with biofilm thickness is in agreement with previous findings for Z-carrier biofilms (Piculell et al., 2016), although lower porosities (approximately of 10 and 30% for Z50 and Z400) were estimated using OCT. Values of biofilm dry density ρ_d (Table 1) for the three biofilms were comparable to that shown in literature (Hu et al., 2013), indicating a higher content of fixed solids in Z500.

< Table 1 >

4.2. Sorption coefficients in biofilms

Sorption was considered significant when a relative concentration drop $(C_{L,0} - C_{L,4h})/C_{L,0}$ higher than 10% was observed (Hörsing et al., 2011), thus accounting for analytical

17

328   uncertainty. Profiles of aqueous concentration of the sorptive micropollutants measured during

329   batch experiments are shown in Fig. 3 (duplicate measurement) and in Fig. S2.

330   Out of the 23 targeted compounds, sorption was significant only for eight micropollutants,

331   namely atenolol, metoprolol, propranolol, citalopram, venlafaxine, erythromycin,

332   clarithromycin and roxithromycin. The presence of chemicals not exhibiting sorption (e.g.,

333   diclofenac and the targeted sulfonamides) suggests that biomass was successfully inhibited

334   during batch experiments, as most targeted compounds were significantly biodegraded in the

335   same MBBRs without biomass inhibition (Torresi et al. 2016). Interestingly, micropollutants

336   that were positively charged (>90% cationic fraction) at the experimental pH of 7.5 presented

337   significant sorption, with exception of sotalol and trimethoprim. Higher sorption potential of

338   positively charged compounds compared to negatively charged or neutral compounds was

339   previously observed for activated sludge biosolids (Stevens-Garmon et al., 2011; Polesel et al.,

340   2015) and soil (Franco and Trapp, 2008).

341

342   *4.2.1. Sorption coefficients $K_{d,eq}$ and comparison with activated sludge*

343   Sorption coefficients $K_{d,eq}$ in Z50, Z200 and Z500 biofilms were calculated for the above listed

344   cationic micropollutants (Table 2). $K_{d,eq}$ values were compared with previously found sorption

345   coefficients in activated sludge, for which the large majority of micropollutant sorption data

346   are available.

347   **< Table 2 >**

348   Values of $K_{d,eq}$ for atenolol at all the three biofilm thickness were up to 2-fold higher than

349   literature values for activated sludge (Radjenović et al., 2009; Stevens-Garmon et al., 2011),

350   while values in Z50 and Z200 were comparable with findings for secondary sludge (Hörsing et

351   al., 2011). As atenolol presents similar molecular properties to other beta-blockers (e.g.,

352 molecular weight, pK_a), the reasons behind this high sorption potential are unclear. As to

353 metoprolol, $K_{d,eq}$ values in Z50, Z200 and Z500 were comparable to previously measured

354 coefficients in activated sludge biomass (Maurer et al., 2007; Sathyamoorthy et al., 2013).

355 Similarly to studies on sludge, propranolol exhibited the highest sorption potential of all

356 selected beta-blockers (Maurer et al., 2007; Radjenović et al., 2009). Notably, a fourth targeted

357 beta blocker sotalol did not show any significant sorption, in agreement with previous findings

358 in activated sludge (Maurer et al., 2007; Sathyamoorthy et al., 2013).

359 Values of $K_{d,eq}$ for Z50 and Z200 were comparable with previous studies on conventional

360 activated sludge and membrane bioreactor (MBR) sludge for clarithromycin (Abegglen et al.,

361 2009; Göbel et al., 2005), erythromycin (Radjenović et al., 2009; Xue et al., 2010) and

362 roxithromycin (Abegglen et al., 2009; Hörsing et al., 2011). On the contrary, $K_{d,eq}$ for Z500

363 differed by one order of magnitude from previously reported values. Nevertheless, 50–80% of

364 dissolved clarithromycin and roxithromycin sorbed on MBR sludge (Abegglen et al., 2009),

365 similarly to clarithromycin and erythromycin in this study (~80%). Furthermore, highly

366 variable macrolide sorption was shown in soil and onto humic acids (Sibley and Pedersen,

367 2008; Uhrich et al., 2014), with estimated $K_{d,eq}$ values also higher than 8 L g^{-1} or 20 L g^{-1},

368 respectively. Macrolides exhibited the highest $K_{d,eq}$ of all sorptive compounds in Z500 but not

369 at lower biofilm thickness (Table 2). This might be related to the low porosity of the biofilms

370 Z50 and Z200. According to Lipinksi's rule of five (Lipinski et al., 1997), macrolides are

371 expected to poorly permeate across cell membranes and thus to move only in the intracellular

372 space (depending on the porosity) due to their high molecular weight (>500 g mol^{-1}).

373 Furthermore, macrolides are mainly excreted in feces (Göbel et al., 2005) and due to

374 protonation of the tertiary amino group, strong ionic interaction of macrolides with the

375 negatively charged surface of the biomass could be expected.

376   Few studies investigated the sorption of the antidepressant venlafaxine and the antiepileptic

377   citalopram. While sorption coefficients for Z50 and Z200 for both compounds are in agreement

378   with existing literature on activated sludge (Hörsing et al., 2011), higher values were found in

379   Z500 for citalopram.

380   In general, sorption coefficients of all the compounds at the three biofilm thicknesses were

381   comparable or higher than values observed with activated sludge biomass. Studies comparing

382   sorption onto MBR sludge and conventional activated sludge biomass (Joss et al., 2006;

383   Abegglen et al., 2009; Reif et al., 2011; Yi and Harper, 2007) revealed a sorption enhancement

384   in the former case. Increased sorption was associated to the smaller size of MBR sludge flocs

385   (assumed to be around 80–300 µm in diameter), thus resulting in higher accessible surface area

386   (Tchobanoglous et al., 2003). In analogy with MBR sludge, it can be postulated that the high

387   accessible surface area in Z-carrier biofilms (related to the biofilm porous structure) may

388   explain the increased sorption capacity of most of the compounds compared to conventional

389   activated sludge biomass.

390

391   *4.2.2. Comparison between $K_{d,eq}$ and $K_{d,4h}$*

392   Sorption coefficients $K_{d,eq}$ were compared with $K_{d,4h}$ values for each chemical and relative

393   deviations Δ (%) between these two coefficients were calculated at different biofilm

394   thicknesses (Table 2) to verify the equilibrium assumption within the experiment duration (4

395   hours). For most compounds, relative deviations for Z50 and Z200 were on average around

396   10%, with the exception of atenolol (>50%). Conversely, Δ values in Z500 were for five

397   compounds higher than 30% (up to 80% for atenolol).

398   Overall, while the assumption of equilibrium reached within 4 h seems justified for Z50 and

399   Z200, diffusive mass transfer can significantly influence observations at higher biofilm

400   thickness. Atenolol was the main exception, for which the 4-h equilibrium assumption seems

401   not valid at any biofilm thickness. On the contrary, propranolol appeared to reach partitioning

402   equilibrium within 4-h in Z50, Z200 and Z500, and similar considerations could be made for

403   citalopram and venlafaxine. Therefore, to reduce uncertainties in sorption experiments,

404   parameter estimation can benefit from calculating the asymptotic aqueous concentration value

405   using e.g., simplified first-order decay equations (Eq. 4).

406

407   *4.2.3. Comparison between $K_{d,eq}$ and $K_{d,sups}$ and trends with biofilm thickness*

408   To assess the impact of biofilm porosity and mass transfer in pores on sorption coefficient

409   estimation, the sorption coefficients $K_{d,eq}$ and $K_{d,susp}$ were compared (Table S4). In Fig. 2, this

410   comparison is presented for two key chemicals (a: metoprolol, b: roxithromycin). For all

411   micropollutants, neglecting the transport from bulk aqueous phase to biofilm pores resulted in

412   an overestimation of sorption coefficients ($K_{d,susp}$ always greater than $K_{d,eq}$). The relative

413   deviation between $K_{d,susp}$ and $K_{d,eq}$ was on average ≤10% for most compounds and 30% for less

414   sorptive compounds (metoprolol and venlafaxine).

415   We further observed that both $K_{d,eq}$ and $K_{d,susp}$ generally increased with increasing biofilm

416   thickness (Fig. 2). Specifically, $K_{d,eq}$ values in Z500 were from 4-fold (most of the compounds)

417   up to 30-fold higher (macrolides antibiotics) than in Z50 (Table 2). It should be highlighted

418   that batch experiments were carried out at the same biomass concentration in the reactors (0.8

419   g L^{-1}). Consequently, the observed $K_{d,eq}$ increase with biofilm thickness likely derives from

420   differences in biofilm composition and/or in its physical properties. Two possible explanations

421   of this observation were proposed:

422   (i) Biomass composition, such as the relative fraction of autotrophic and heterotrophic bacteria

423   and/or the content of extracellular polymeric substances (EPS), can influence sorption

424   properties. EPS protein content was previously positively correlated with K_d for aromatic

425   chemicals in untreated and treated sewage sludge and colloids (Barret et al., 2010) and for the

426   estrogen EE2 and trimethoprim in nitrifying and heterotrophic biomass (Khunjar and Love,

427   2011). Bassin et al., (2012) further observed higher concentration of proteins and

428   polysaccharides (that mainly compose EPS) in heterotrophic MBBRs than in nitrifying

429   MBBRs. Higher fractions of heterotrophic bacteria (determined using quantitative PCR of 16S

430   rRNA) were measured in Z200 and Z500 compared to Z50 (Torresi et al., 2016), possibly

431   justifying the increased sorption capacity in thicker biofilms (Z200, Z500). Further

432   investigation on the EPS content in the different biofilms is thus required to support this

433   hypothesis, given the key role of EPS in the sorption of neutral and ionizable organic

434   chemicals (Späth et al., 1998; Barret et al., 2010; Khunjar and Love, 2011).

435   (ii)   Porosity can influence the available surface area inside the biofilm. Sorption has been

436   previously positively impacted by reduced particle size, i.e., greater surface area, in suspended

437   biomass (Khunjar and Love, 2011) and biomass floc suspension derived from MBRs (Yi and

438   Harper, 2007). Thicker biofilms, having lower biomass density and substantially higher

439   porosity than thin biofilms, could accordingly provide for higher available surface (and thus

440   more accessible sites) for solid-liquid partitioning.

441   Finally, $K_{d,eq}$ values were normalized to the highest value of $K_{d,eq}$ (i.e., for Z500, $K_{d,eqZ500}$). The

442   obtained profiles followed two distinct trends as a function of biofilm thickness (Fig. 2c–d): (i)

443   beta-blockers and venlafaxine, exhibiting a logarithmic-like increase between Z50 and Z500;

444   and (ii) macrolides and citalopram, presenting significantly higher values for Z500, thus an

445   exponential-like increase of $K_{d,eq}$ with thickness. The question arises as to the influence of the

446   specific chemical properties of micropollutants on partitioning in biofilms, which was further

447   assessed using correlation analysis (see 4.5.2).

448   < **Figure 2** >

449

450   *4.3. Modelling diffusion and sorption in biofilm*

451   Based on the considerations above, calculated $K_{d,eq}$ were used to calibrate the diffusion-

452   sorption model against experimental data for the estimation of the dimensionless effective

453   diffusivity coefficient *f* (the only parameter estimated with the model). Simulated aqueous

454   concentrations (continuous lines, Fig. 3) predicted reasonably well the measured

455   concentrations in bulk liquid (circles, Fig. 3) for most of the targeted compounds (i.e., for

456   propranolol, clarithromycin, erythromycin, roxithromycin, citalopram, venlafaxine $R^2 > 0.9$;

457   Table S5). For atenolol, measured concentrations were less well predicted for Z50 and Z500

458   (R^2 equal to 0.8).

459   The simulated micropollutant concentrations in the bulk liquid and in the biofilm pores liquid

460   (dashed lines, Fig. 3) should converge when partitioning equilibrium is reached. This

461   equilibrium condition was satisfied for most compounds in Z50 and Z200 within 4 h

462   experimental time, with an average 10% relative deviation between simulated concentrations in

463   bulk and in biofilm pores. For the thickest biofilm (Z500), however, model predictions for

464   most of targeted chemicals suggested that equilibrium was not reached within 4 h (60%

465   average discrepancy with the last measurement). It is likely that, due to the greater thickness,

466   increased time to diffuse in deeper biofilm and thus to achieve sorption equilibrium is required

467   in Z500. The exception was propranolol, for which equilibrium seemed to be reached in all the

468   three biofilms, thus supporting results (relative deviation between $K_{d,4h}$ and $K_{d,eq}$) presented in

469   Table 2. For macrolide antibiotics, this discrepancy was significant and simulation results

470   suggested a time for partitioning equilibrium of approximately 10 days—in good agreement

471   with equilibrium times (days, months and years) in other environmental matrices (Delle Site,

472 2001). Furthermore, the large molecular volume and weight of macrolides (2- to 3-fold higher

473 than the other targeted compounds, Table S2), as well as their high sorption potential in Z500,

474 suggest slower diffusive transport inside the biofilm, as previously observed for hydrophobic

475 organic molecules in sediments and soil (Wu and Gschwend, 1986).

476 There is a large variability concerning the time to reach partitioning equilibrium for organic

477 chemicals in biofilms (Alvarino et al., 2015; Headley et al., 1998; Shi et al., 2011; Wicke et

478 al., 2008; Writer et al., 2011), with values ranging from, e.g., 4 to 80 h for biofilm of 0.1 mm

479 thickness (Wicke et al., 2008). In conclusion, our observations conflict with the widely held

480 assumption of significantly shorter period of time (i.e. minutes to 1–2 hours) necessary to

481 reach equilibrium in activated sludge (e.g., Hörsing et al., 2011; Pomiès et al., 2013). This may

482 be explained by differences in pore-scale (hydro)dynamic conditions in MBBRs and activated

483 sludge reactors, resulting in more pronounced mass transfer limitation in MBBRs.

484   **< Figure 3 >**

485

486 ***4.4. Influence of biofilm and chemical properties on diffusion (f) and partitioning ($K_{d,eq}$)***

487 *4.4.1. Estimation of f and proposed empirical correlation*

488 Values of the dimensionless effective diffusivity coefficient *f* estimated for the three biofilm

489 thicknesses and the eight sorptive compounds are reported in Fig. 4. For most of the

490 compounds, with the exception of roxithromycin, *f* decreased with biofilm density and thus

491 increased with biofilm thickness and porosity (with *f* in Z500 significantly higher than in Z200

492 and Z50 for all the compounds, and *f* in Z200 significantly higher than Z50 for six

493 compounds). In thinner biofilms (≤ 50 μm), the transport of micropollutants could thus be

494 limited by the high biomass density and the reduced porosity. A number of regressions to

495 estimate *f* of solutes in biofilms as a function of biofilm density or porosity have been

24

496 previously developed (Fan et al., 1990; Guimerà et al., 2016; Horn and Morgenroth, 2006;

497 Zhang and Bishop, 1994a), suggesting a negative correlation between f and density. Selected

498 regression profiles (i.e., Guimerà et al., 2016; Horn and Morgenroth, 2006; Zhang and Bishop,

499 1994a; see Table S6) are reported in Fig. S3 for comparison with our f estimations. In

500 particular, Guimerá et al. (2016) observed strong mass transfer limitation ($f < 0.1$) for oxygen

501 in biofilm with density greater than 50 gVSS L^{-1}, in close agreement with findings (specifically

502 for Z50) presented in this study.

503 **< Figure 4 >**

504 In general, estimated f were lower than values calculated from proposed regressions (Guimerà

505 et al., 2016; Horn and Morgenroth, 2006; Zhang and Bishop, 1994a) (Fig. S3). While these

506 regressions were identified for solutes with lower molecular weight (< 100 g mol^{-1}) and high

507 solubility (e.g., O$_2$, sodium chloride, sodium nitrate), lower values of f (~0.2) were reported for

508 most organic solutes with larger molecular weight (e.g., sugars and fatty acids; Stewart, 2003,

509 1998).

510 Given the possible influence of chemical properties on micropollutant diffusivity, we evaluated

511 the relationship between f and several physico-chemical descriptors (section 3.5). No specific

512 correlation was observed between f and molecular volume and other descriptors (Fig. S4). We

513 observed a positive correlation only between f and logK_{OW} of the targeted compounds (Fig.

514 S5), while negative dependence was reported in literature for organic compounds (Headley et

515 al., 1998; Wicke et al., 2007; Wu and Gschwend, 1986). Notably, in this study the correlation

516 was found for less hydrophobic ($0.1 < \log K_{OW} < 3.7$) and positively charged compounds

517 (differently from previous studies), for which electrostatic interactions may also have

518 influenced transport and partitioning. Thus, an empirical correlation between f, biofilm density

519 ρ (as function of biofilm thickness) and log K_{OW} is proposed (Eq. 7):

520 $$f = \frac{1}{488 \cdot e^{-0.0072 L_F}} \ln\left(\frac{-12.7 - \log K_{OW,\max}}{\log K_{ow} - \log K_{OW,\max}}\right) \qquad \text{(Eq. 7)}$$

521 where L_F is the biofilm thickness (µm) and log $K_{OW,max}$ is the asymptotic log K_{OW}

522 approximating the highest value for the compounds selected. Profiles of f deriving from Eq. 7

523 were then depicted in Fig. 5, along with the estimated f values for the three biofilm thickness

524 (symbols, see also Fig. 4). Further details on the formulation of Eq. 7 are given in the SI

525 (section S4). We note that the size of the available data set may not be sufficiently large to

526 validate the correlation, and additional experimental evidence (higher biofilm thickness, wider

527 range of log K_{OW}) may be required for further confirmation.

528   **< Figure 5 >**

529

530 *4.4.2. Predictors of micropollutant $K_{d,eq}$ in biofilms*

531 Correlation analyses were performed between $K_{d,eq}$ and a number of physico-chemical

532 micropollutant descriptors.

533 First, the octanol-water partitioning coefficient of the neutral species (logK_{OW}) and the species-

534 dependent octanol-water distribution coefficient (log$D$) were assessed, exhibiting insignificant

535 correlation with $K_{d,eq}$ (-0.27 < Pearson's r < 0.15 for the three biofilms). This finding confirms

536 the limited reliability of logK_{OW} and log$D$ as sorption predictors for organic cations, as

537 previously shown in soil (Tolls, 2001; Franco and Trapp, 2008; Droge and Gross, 2013a).

538 Following this preliminary assessment, correlations with physico-chemical descriptors for

539 ionizable compounds (i.e., logpK_a, nrB, MV, log$TPSA$, log$vdWA$, V_X) were investigated (Fig. 6

540 and S6). Correlations for biofilm Z50 was performed only considering six compounds ($K_{d,eq}$ =

541 0 for venlafaxine and roxithromycin).

26

542 No significant correlations were found with the stereochemistry parameter *nRB* and log*pK$_a$*

543 (Fig.S6). While previous studies positively correlated the sorption of cationic compounds with

544 *pK$_a$* (r^2=0.5) (Franco and Trapp, 2008), the narrow range of *pK$_a$* values covered in this study

545 prevented us from concluding on the significance of this indicator.

546 Interestingly, our analysis revealed a significant positive correlation only for Z500 between

547 log*K$_{d,eq}$* and log*TPSA*, log*vdWA,* McGowan's *V$_X$* (Fig. 6) and *MV* (Fig. S6a). The parameter

548 *TPSA* was previously identified as sorption predictor only for neutral and negatively charged

549 compounds, although with a negative correlation (Sathyamoorthy and Ramsburg, 2013). *TPSA*

550 reflects the polarity of the organic chemical by accounting for the oxygen and nitrogen atoms

551 as well as attached hydrogen atoms, and increased polar surface area has been associated to

552 reduced absorption and cell permeability of pharmaceuticals in humans (Palm et al., 1997; Ertl

553 et al., 2000). Hence, the significant correlation with log*K$_{d,eq}$* may suggest (at least for thicker

554 biofilm) a positive influence of polarity on the retention of cations in biofilm, possibly

555 resulting from the improved accessibility to deeper biofilm through transport in the

556 intracellular space.

557

558 On the other hand, the positive correlation of log*K$_{d,eq}$* with log*vdWA*, *MV* and *V$_X$* still suggests

559 a contribution of hydrophobicity in sorption of positively charged compounds in Z500 biofilm.

560 This finding is in line with previously established regressions for the prediction of distribution

561 coefficients based on van der Waals volume (Kamlet et al., 1998) or *V$_X$* (Abraham, 1993;

562 Abraham and Acree, 2010; Droge and Goss, 2013a,b,c) for neutral and ionized molecules.

563 Notably, McGowan's volume positively correlates with van der Waals volume (Zhao et al.,

564 2003), which is itself correlated to *vdWA*. Hence, both *vdWA* and *V$_X$* provide an indication of

565 the influence of the molecular size in the cavity formation mechanism, through which solute

27

566   molecules can distribute to an organic phase at the expenses of (i.e., by replacing) water

567   molecules (Mackay and Vasudevan, 2012).

568   Considering the relevance of the correlation between $\log K_{d,\text{eq}}$ and V_X for Z500, an empirical

569   regression model (Eq. 8) was tested based on the equation previously proposed by Droge and

570   Goss (2013a,c) for sorption prediction of organic cations to soil organic matter:

571     $\log K_{d,eq} = a \cdot V_X / 100 + b \cdot NA_i + c$ (Eq. 8)

572   where $K_{d,eq}$ is expressed in L kg^{-1} and NA_i indicates the number of hydrogen atoms bound to the

573   charged nitrogen moiety. The coefficients a, b and c were estimated by fitting Eq. 8 to

574   measured sorption coefficients. The comparison between predicted and measured $\log K_{d,eq}$ for

575   Z500 is shown in Fig. 6d (a=0.35; b=0.45; c=1.48). The regression ($r^2 = 0.58$) could only

576   partly describe sorption of cationic micropollutants in Z500 biofilms, yielding rather good $K_{d,eq}$

577   predictions (within factor 1.5 from measurements) for propranolol, clarithromycin,

578   erythromycin and roxythromycin. Potential improvement of sorption predictions may be

579   expected from the identification of correction factors for polar functional groups—an area

580   beyond the scope of this study due to the limited number of substances.

581   Overall, results from this assessment confirm the challenges in the identification of unique and

582   reliable sorption predictors for positively charged micropollutants in biofilm, as previously

583   recognized for other matrices (Kah and Brown, 2007; Franco and Trapp, 2008; Franco et al.,

584   2009; Sathyamoorthy and Ramsburg, 2013; Droge and Goss, 2013a,c; Bittermann et al., 2016).

585   Nevertheless, it should be highlighted that in this study sorption was consistently observed

586   only for positively charged compounds, indicating that electrostatic interaction with negatively

587   charged biomass surfaces play a major role for sorption in biofilms.

588   **< Figure 6 >**

589

590 **5. Conclusions**

591 This study investigated the sorption and the diffusion of selected micropollutants in nitrifying

592 MBBR biofilms (thickness=50, 200, 500 µm) by means of targeted experiments and process

593 modelling, leading to the following conclusions:

594 • Sorption in biofilm occurred only for eight positively charged micropollutants (i.e.,

595 three macrolides, three beta-blockers and two psycho-active pharmaceuticals) out of 23

596 targeted substances. Electrostatic interaction with the negatively charged biomass

597 surfaces appears to play a major role in the sorption to biofilms.

598 • Values of the partitioning coefficient $K_{d,eq}$ increased with increasing biofilm thickness

599 for most of the sorbed compounds, being related to the increasing biofilm porosity and

600 thus the higher surface area accessible for sorption. Sorption equilibria were reached

601 within the duration of sorption experiments (4 h) for a number of compounds in 50 and

602 200 µm thick biofilms, but not in the thickest biofilm. Slower equilibrium in thick

603 biofilms (≥500 µm) is likely determined by the longer time required to diffuse in deeper

604 biofilm.

605 • Dimensionless effective diffusivity coefficients f for micropollutants (estimated for the

606 first time in wastewater treatment biofilms) were negatively correlated with biofilm

607 density, while showing an increase with increasing porosity. This indicates that

608 diffusive transport may be strongly limited by the higher biomass density (and the

609 lower porosity) of thinner biofilms.

610 • Significant positive correlations were observed between $logK_{d,eq}$ and a limited number

611 of chemical properties of micropollutants (topological polar surface area, van der Waals

612 area and McGowan´s volume) but not for all biofilm thicknesses, confirming the

613 challenges in the prediction of sorption in biofilms and other matrices for positively

29

614   charged compounds.

615

616   **Acknowledgments**

References

621

622 Abegglen, C., Joss, A., McArdell, C.S., Fink, G., Schlüsener, M.P., Ternes, T.A., Siegrist, H.,

623   2009. The fate of selected micropollutants in a single-house MBR. Water Res. 43, 2036–

624   46.

625 Abraham, M.H., McGowan, J.C., 1987. The use of characteristic volumes to measure cavity

626   terms in reversed phase liquid chromatography. Chromatogr. 23, 243–246.

627 Abraham, M.H., 1993. Scales of solute hydrogen-bonding: Their construction and application

628   to physicochemical and biochemical processes. Chem. Soc. Rev. 22, 73–83.

629 Abraham, M.H., Acree Jr., W.E., 2010. Equations for the transfer of neutral molecules and

630   ionic species from water to organic phases. J. Org. Chem. 75, 1006–1015

631 Alvarino, T., Suarez, S., Katsou, E., Vazquez-Padin, J., Lema, J.M., Omil, F., 2015. Removal

632   of PPCPs from the sludge supernatant in a one stage nitritation/anammox process. Water

633   Res. 68, 701–709.

634 Andersen, H.R., Hansen, M., Kjølholt, J., Stuer-Lauridsen, F., Ternes, T., Halling- Sørensen,

635   B., 2005. Assessment of the importance of sorption for steroid estrogens removal during

636   activated sludge treatment. Chemosphere 61, 139–146.

637 Barret, M., Carrère, H., Latrille, E., Wisniewski, C., Patureau, D., 2010. Micropollutant and

638   sludge characterization for modeling sorption equilibria. Environ. Sci. Technol. 44, 1100–

639   1106.

640 Barret, M., Carrere, H., Patau, M., Patureau, D., 2011. Kinetics and reversibility of

641   micropollutant sorption in sludge. J. Environ. Monit. 13, 2770–2774.

642 Bassin, J.P., Kleerebezem, R., Rosado, A.S., van Loosdrecht, M.C.M., Dezotti, M., 2012.

643   Effect of different operational conditions on biofilm development, nitrification, and

644   nitrifying microbial population in moving-bed biofilm reactors. Environ. Sci. Technol. 46,

645   1546–1555.

646   Beyenal, H., Lewandowski, Z., 2005. Modeling mass transport and microbial activity in

647   stratified biofilms. Chem. Eng. Sci. 60, 4337–4348.

648   Berthod, L., Whitley, D.C., Roberts, G., Sharpe, A., Greenwood, R., Mills, G.A., 2017.

649   Quantitative structure-property relationships for predicting sorption of pharmaceuticals to

650   sewage sludge during waste water treatment processes. Sci. Total Environ. 579, 1512–

651   1520.

652   Bittermann, K., Spycher, S., Goss, K.U., 2016. Comparison of different models predicting the

653   phospholipid-membrane water partition coefficients of charged compounds. Chemosphere

654   144, 382–391.

655   Brockmann, D., Rosenwinkel, K.H., Morgenroth, E., 2008. Practical identifiability of

656   biokinetic parameters of a model describing two-step nitrification in biofilms. Biotechnol.

657   Bioeng. 101, 497–514.

658   Clesceri, L.S., 1989. Standard methods for the examination of water and wastewater. American

659   Public Health Association.

660   Converti, A., Del Borghi, M., Zilli, M., 1997. Evaluation of phenol diffusivity through

661   Pseudomonas putida biofilms: Application to the study of mass velocity distribution in a

662   biofilter. Bioprocess Eng. 16, 105–114.

663   Cumming, G., Fidler, F., Vaux, D.L., 2007. Error bars in experimental biology. J. Cell Biol.

664   177, 7–11.

665   Delle Site, A., 2001. Factors affecting sorption of organic compounds in natural sorbent/water

666   systems and sorption coefficients for selected pollutants. A review. J. Phys. Chem. Ref.

667   Data 30, 187–439.

668   Droge, S.T.J., Goss, K.U., 2013a. Ion-exchange affinity of organic cations to natural organic

669   matter: Influence of amine type and nonionic interactions at two different pHs. Environ.

670   Sci. Technol. 47, 798–806.

671   Droge, S.T.J., Goss, K.U., 2013b. Sorption of organic cations to phyllosilicate clay minerals:

672   CEC normalization, salt dependency, and the role of electrostatic and hydrophobic effects.

673   Environ. Sci. Technol. 47, 14224–14232.

674   Droge, S.T.J., Goss, K.U., 2013c. Development and evaluation of a new sorption model for

675   organic cations in soil: Contributions from organic matter and clay minerals. Environ. Sci.

676   Technol. 47, 14233–14241.

677   Ertl, P., Rohe, B., Selzer, P., 2000. Fast calculation of molecular polar surface area as sum of

678   fragment-based contributions and its application to the prediction of drug transport

679   properties. J. Med. Chem. 43, 3714–3717.

680   Escolà Casas, M.E., Chhetri, R.K., Ooi, G., Hansen, K.M.S., Litty, K., Christensson, M.,

681   Kragelund, C., Andersen, H.R., Bester, K., 2015. Biodegradation of pharmaceuticals in

682   hospital wastewater by staged Moving Bed Biofilm Reactors (MBBR). Water Res. 83,

683   293–302.

684   Falås, P., Longrée, P., la Cour Jansen, J., Siegrist, H., Hollender, J., Joss, A, 2013.

685   Micropollutant removal by attached and suspended growth in a hybrid biofilm-activated

686   sludge process. Water Res. 47, 4498–4506.

687   Fan, L.S., Leyva-Ramos, R., Wisecarver, K.D., Zehner, B.J., 1990. Diffusion of phenol

688   through a biofilm grown on activated carbon particles in a draft-tube three-phase

689   fluidized-bed bioreactor. Biotechnol. Bioeng. 35, 279–286.

690   Fernandez-Fontaina, E., Omil, F., Lema, J.M., Carballa, M., 2012. Influence of nitrifying

691   conditions on the biodegradation and sorption of emerging micropollutants. Water Res.

692   46, 5434–5444.

693   Franco, A., Fu, W., Trapp, S., 2009. Influence of soil pH on the sorption of ionizable

694   chemicals: modeling advances. Environ. Toxicol. Chem. 28, 458–464.

695   Franco, A., Struijs, J., Gouin, T., Price, O.R., 2013. Evolution of the sewage treatment plant

696   model SimpleTreat: Applicability domain and data requirements. Integr. Environ. Assess.

697   Manag. 9, 1–32.

698   Franco, A., Trapp, S., 2008. Estimation of the soil-water partition coefficient normalized to

699   organic carbon for ionizable organic chemicals. Environ. Toxicol. Chem. 27, 1995–2004.

700   Göbel, A., Thomsen, A., McArdell, C.S., Joss, A., Giger, W., 2005. Occurrence and sorption

701   behavior of sulfonamides, macrolides, and trimethoprim in activated sludge treatment.

702   Environ. Sci. Technol. 39, 3981–3989.

703   Guimerà, X., Dorado, A.D., Bonsfills, A., Gabriel, G., Gabriel, D., Gamisans, X., 2016.

704   Dynamic characterization of external and internal mass transport in heterotrophic biofilms

705   from microsensors measurements. Water Res. 102, 551–560.

706   Hamon, P., Villain, M., Marrot, B., 2014. Determination of sorption properties of

707   micropollutants: What is the most suitable activated sludge inhibition technique to

708   preserve the biomass structure? Chem. Eng. J. 242, 260–268.

709   Hayduk, W., Laudie, H., 1974. Prediction of diffusion coefficients for nonelectrolytes in dilute

710   aqueous solutions. AIChE J. 20, 611–615.

711   Headley, J. V., Gandrass, J., Kuballa, J., Peru, K.M., Gong, Y., 1998. Rates of sorption and

712   partitioning of contaminants in river biofilm. Environ. Sci. Technol. 32, 3968–3973.

713   Holden, P.A., Hunt, J.R., Firestone, M.K., 1997. Toluene diffusion and reaction in unsaturated

714   Pseudomonas putida biofilms. Biotechnol. Bioeng. 56, 656–670.

715   Horn, H., Morgenroth, E., 2006. Transport of oxygen, sodium chloride, and sodium nitrate in

716   biofilms. Chem. Eng. Sci. 61, 1347–1356.

717   Hörsing, M., Ledin, A., Grabic, R., Fick, J., Tysklind, M., Jansen, J. la C., Andersen, H.R.,

718   2011. Determination of sorption of seventy-five pharmaceuticals in sewage sludge. Water

719   Res. 45, 4470–4482.

720   Hu, M., Zhang, T.C., Stansbury, J., Neal, J., Garboczi, E.J., 2013. Determination of porosity

721   and thickness of biofilm attached on irregular-shaped media. J. Environ. Eng. 139, 923–

722   931.

723   Hyland, K.C., Dickenson, E.R. V, Drewes, J.E., Higgins, C.P., 2012. Sorption of ionized and

724   neutral emerging trace organic compounds onto activated sludge from different

725   wastewater treatment configurations. Water Res. 46, 1958–1968.

726   Joss, A., Andersen, H., Ternes, T., Richle, P.R., Siegrist, H., 2004. Removal of estrogens in

727   municipal wastewater treatment under aerobic and anaerobic conditions: consequences for

728   plant optimization. Environ. Sci. Technol. 38, 3047–3055.

729   Joss, A., Zabczynski, S., Göbel, A., Hoffmann, B., Löffler, D., McArdell, C.S., Ternes, T. a.,

730   Thomsen, A., Siegrist, H., 2006. Biological degradation of pharmaceuticals in municipal

731   wastewater treatment: Proposing a classification scheme. Water Res. 40, 1686–1696.

732   Kah, M., Brown, C.D., 2007. Prediction of the adsorption of Ionizable pesticides in soils. J.

733   Agric. Food Chem. 55, 2312–2322.

734   Kamlet, M.J., Doherty, R.M., Abraham, M.H., Marcus, Y., Taft, R.W., 1988. Linear solvation

735   energy relationships. 46. An improved equation for correlation and prediction of

736   octanol/water partition coefficients of organic nonelectrolytes (including strong hydrogen

737   bond donor solutes). J. Phys. Chem. 92, 5244–5255.

738   Khunjar, W.O., Love, N.G., 2011. Sorption of carbamazepine, 17α-ethinylestradiol, iopromide

739   and trimethoprim to biomass involves interactions with exocellular polymeric substances.

740   Chemosphere 82, 917–922.

741   Lipinski, C.A., Lombardo, F., Dominy, B.W., Feeney, P.J., 1997. Experimental and

742   Computational Approaches to Estimate Solubility and Permeability in Drug Discovery

743   and Develop ment Settings. Adv. Drug Deliv. Rev. 23, 3–25.

744   Margot, J., Rossi, L., Barry, D.A., Holliger, C., 2015. A review of the fate of micropollutants

745   in wastewater treatment plants. Wiley Interdiscip. Rev. Water 2, 457–487.

746   Maurer, M., Escher, B.I., Richle, P., Schaffner, C., Alder, a C., 2007. Elimination of beta-

747   blockers in sewage treatment plants. Water Res. 41, 1614–1622.

748   Mackay, A.A., Vasudevan, D., 2012. Polyfunctional ionogenic compound sorption: Challenges

749   and new approaches to advance predictive models. Environ. Sci. Technol. 46, 9209–9223.

750   Ort, C., Gujer, W., 2008. Sorption and high dynamics of micropollutants in sewers. Water Sci.

751   Technol. 57, 1791–1797.

752   Palm, K., Stenberg, P., Luthman, K., Artursson, P., 1997. Polar molecular surface properties

753   predict the intestinal absorption of drugs in humans. Pharm. Res. 14, 568–571.

754   Piculell, M., Suarez, C., Li, C., Christensson, M., Persson, F., Wagner, M., Hermansson, M.,

755   Jonsson, K., Welander, T., 2016. The inhibitory effects of reject water on nitrifying

756   populations grown at different biofilm thickness. Water Res. 104, 292–302.

757   Plósz, B.G., Langford, K.H., Thomas, K. V, 2012. An activated sludge modeling framework

758   for xenobiotic trace chemicals (ASM-X): assessment of diclofenac and carbamazepine.

759   Biotechnol. Bioeng. 109, 2757–2769.

760   Plósz, B.G.Y., Leknes, H., Thomas, K. V, 2010. Impacts of competitive inhibition, parent

761   compound formation and partitioning behavior on the removal of antibiotics in municipal

762   wastewater treatment. Environ. Sci. Technol. 44, 734–742.

763   Polesel, F., Lehnberg, K., Dott, W., Trapp, S., Thomas, K. V, Plósz, B.G., 2015. Factors

764   influencing sorption of ciprofloxacin onto activated sludge: Experimental assessment and

765   modelling implications. Chemosphere 119, 105–111.

766   Pomiès, M., Choubert, J.-M., Wisniewski, C., Coquery, M., 2013. Modelling of micropollutant

767   removal in biological wastewater treatments: a review. Sci. Total Environ. 443, 733–748.

768   Radjenović, J., Petrović, M., Barceló, D., 2009. Fate and distribution of pharmaceuticals in

769   wastewater and sewage sludge of the conventional activated sludge (CAS) and advanced

770   membrane bioreactor (MBR) treatment. Water Res. 43, 831–841.

771   Rattier, M., Reungoat, J., Keller, J., Gernjak, W., 2014. ScienceDirect Removal of

772   micropollutants during tertiary wastewater treatment by biofiltration : Role of nitrifiers

773   and removal mechanisms. Water Res. 54, 89–99.

774   Reichert, P., 1994. Aquasim - a tool for simulation and data-analysis of aquatic systems. Water

775   Sci. Technol. 30, 21–30.

776   Reif, R., Besancon, A., Le Corre, K., Jefferson, B., Lema, J.M., Omil, F., 2011. Comparison of

777   PPCPs removal on a parallel-operated MBR and AS system and evaluation of effluent

778   post-treatment on vertical flow reed beds. Water Sci. Technol. 63, 2411–2417.

779   Sathyamoorthy, S., Ramsburg, C.A., 2013. Assessment of quantitative structural property

780   relationships for prediction of pharmaceutical sorption during biological wastewater

781   treatment. Chemosphere 92, 639–646.

782   Shi, Y.J., Wang, X.H., Qi, Z., Diao, M.H., Gao, M.M., Xing, S.F., Wang, S.G., Zhao, X.C.,

783   2011. Sorption and biodegradation of tetracycline by nitrifying granules and the toxicity

784   of tetracycline on granules. J. Hazard. Mater. 191, 103–109.

785   Sibley, S.D., Pedersen, J.A., 2008. Interaction of the macrolide antimicrobial clarithromycin

786   with dissolved humic acid. Environ. Sci. Technol. 42, 422–428.

787   Späth, R., Flemming, H.C., Wuertz, S. (1998). Sorption properties of biofilms. Water Sci.

788   Technol. 37, 207–210.

789   Stevens-Garmon, J., Drewes, J.E., Khan, S.J., McDonald, J.A., Dickenson, E.R. V, 2011.

790   Sorption of emerging trace organic compounds onto wastewater sludge solids. Water Res.

791   45, 3417–3426.

792   Stewart, P.S., 2003. Diffusion in Biofilms: why is diffusion an important process. J. Bacteriol.

793   185, 1485–1491.

794   Stewart, P.S., 1998. A review of experimental measurements of effective diffusive

795   permeabilities and effective diffusion coefficients in biofilms. Biotechnol. Bioeng. 59,

796   261–272.

797   Tchobanoglous G., Burton F., Stensel H., Wastewater Engineering: Treatment and Reuse, 4th

798   ed., Metcalf and Eddy, Inc., McGraw-Hill Company, New York, 2003.

799   Ternes, T.A., Herrmann, N., Bonerz, M., Knacker, T., Siegrist, H., Joss, A., 2004. A rapid

800   method to measure the solid-water distribution coefficient (K_d) for pharmaceuticals and

801   musk fragrances in sewage sludge. Water Res. 38, 4075–4084.

802   Tolls, J. (2001). Sorption of veterinary pharmaceuticals in soils: A review. Environ. Sci.

803   Technol. 35, 3397–3406

804   Torresi, E., Fowler, S.J., Polesel, F., Bester, K., Andersen, H.R., Smets, B.F., Plósz, B.G.,

805   Christensson, M., 2016. Biofilm Thickness Influences Biodiversity in Nitrifying

806   MBBRs—Implications on Micropollutant Removal. Environ. Sci. Technol., 50 (17),

807   9279–9288.

808   Tran, N.H., Urase, T., Kusakabe, O., 2009. The characteristics of enriched nitrifier culture in

809   the degradation of selected pharmaceutically active compounds. J. Hazard. Mater. 171,

810   1051–1057.

811   Trapp, S., Matthies, M., 1998. Transport and Transformation of Compounds in Soil, in:

812   Chemodynamics and Environmental Modeling. Springer-Verlag, Berlin, Germany.

813   Uhrich, S.R.W., Navarro, D.A., Zimmerman, L., Aga, D.S., 2014. Assessing antibiotic sorption

814   in soil: A literature review and new case studies on sulfonamides and macrolides. Chem.

815   Cent. J. 8, 1–12.

816   Vasiliadou, I.A., Molina, R., Martínez, F., Melero, J. a, 2014. Experimental and modeling

817   study on removal of pharmaceutically active compounds in rotating biological contactors.

818   J. Hazard. Mater. 274, 473–482.

819   Wanner, O., Reichert, P., 1996. Mathematical modeling of mixed-culture biofilms. Biotechnol.

820   Bioeng. 49, 172–184.

821   Wicke, D., Böckelmann, U., Reemtsma, T., 2007. Experimental and modeling approach to

822   study sorption of dissolved hydrophobic organic contaminants to microbial biofilms.

823   Water Res. 41, 2202–2210.

824   Wicke, D., Böckelmann, U., Reemtsma, T., 2008. Environmental influences on the partitioning

825   and diffusion of hydrophobic organic contaminants in microbial biofilms. Environ. Sci.

826   Technol. 42, 1990–1996.

827   Writer, J.H., Ryan, J.N., Barber, L.B., 2011. Role of biofilms in sorptive removal of steroidal

828   hormones and 4-nonylphenol compounds from streams. Environ. Sci. Technol. 45, 7275–

829   7283.

830   Wu, S.C., Gschwend, P.M., 1986. Sorption kinetics of hydrophobic organic compounds to

831   natural sediments and soils. Environ. Sci. Technol. 20, 717–725.

832   Wunder, D.B., Bosscher, V.A., Cok, R.C., Hozalski, R.M., 2011. Sorption of antibiotics to

833   biofilm. Water Res. 45, 2270–2280.

834   Xue, W., Wu, C., Xiao, K., Huang, X., Zhou, H., Tsuno, H., Tanaka, H., 2010. Elimination and

835   fate of selected micro-organic pollutants in a full-scale anaerobic/anoxic/aerobic process

836   combined with membrane bioreactor for municipal wastewater reclamation. Water Res.

837   44, 5999–6010.

838   Yi, T., Harper, W.F., 2007. The effect of biomass characteristics on the partitioning and
839   sorption hysteresis of 17alpha-ethinylestradiol. Water Res. 41, 1543–1553.

840   Zacarias, G.D., Ferreira, C.P., Velasco-Hernandez, J.X., 2005. Porosity and tortuosity relations
841   as revealed by a mathematical model of biofilm structure. J. Theor. Biol. 233, 245–251.

842   Zhang, S.F., Splendiani, A., Freitas dos Santos, L.M., Livingston, A.G., 1998. Determination
843   of pollutant diffusion coefficients in naturally formed biofilms using a single tube
844   extractive membrane bioreactor. Biotechnol. Bioeng. 59, 80–89.

845   Zhang, T.C., Bishop, P.L., 1994a. Evaluation of turtuosity factors and effective diffusivities in
846   biofilms. Water Res. 28, 2279–2287.

847   Zhang, T.C., Bishop, P.L., 1994c. Density, porosity, and pore structure of biofilms. Water Res.
848   28, 2267–2277.

849   Zhao, Y.H., Abraham, M.H., Zissimos, A.M., 2003. Determination of McGowan volumes for
850   ions and correlation with van der Waals volumes. J. Chem. Inf. Comput. Sci. 43, 1848–
851   1854.

Table 1. Biofilm characteristics and input parameters used in the sorption and diffusion model in this study. The parameter ρ_d denotes the dry mass of biofilm per volume of dry biofilm (defining a true density), while ρ denotes the dry mass of (microbial) biomass per volume of wet biofilm (defining the concentration of biomass within the biofilm). TAS defines total attached solids.

Parameter	Z50	Z200	Z500	Reference
Dry biofilm mass per carrier (gTAS m^{-2})	2.6 ± 0.2	4.0 ± 0.3	8.0 ± 0.6	Measured
Biofilm dry density ρ_d (g cm^{-3})	1.05 ± 0.09	1.05 ± 0.07	1.17 ± 0.05	Calculated
Biomass density in wet biofilm ρ (kg m^{-3})	51.9 ± 2.6	20.0 ± 1.3	16.0 ± 0.8	Calculated
Porosity ε (%)	75 ± 4	91 ± 6	93 ± 7	Calculated
Biomass concentration in batch reactor (gTAS L^{-1})	0.80 ± 0.07	0.78 ± 0.06	0.78 ± 0.03	Measured

1

Table 2. Sorption coefficients calculated using the asymptotic equilibrium concentration ($K_{d,eq}$, L g^{-1}; mean and standard deviation are given) and the last measured aqueous concentration (t=4 h) during batch experiments ($K_{d,4h}$, L g^{-1}) for eight of the 23 spiked chemical compounds. The parameter Δ (%) defines the relative deviation between the two K_d values, providing also an indication of the deviation from partitioning equilibrium. Literature K_d values comprise measured partition coefficients in conventional activated sludge and membrane bioreactor (MBR) sludge.

	Z50			Z200			Z500			
	$K_{d,eq}$ (L g^{-1})	$K_{d,4h}$ (L g^{-1})	Δ (%)	$K_{d,eq}$ (L g^{-1})	$K_{d,4h}$ (L g^{-1})	Δ (%)	$K_{d,eq}$ (L g^{-1})	$K_{d,4h}$ (L g^{-1})	Δ (%)	Literature K_d (L g^{-1})
Atenolol	1.12±2.21	0.26	77	1.12±0.34	0.68	38	4.84±0.73	0.95	80	(0.006)[1]–1.9[2]
Metoprolol	0.08±0.01	0.08	3	0.19±0.06	0.16	15	0.28±0.02	0.15	44	<0.01[3]–0.23[4]
Propranolol	0.50±0.04	0.54	-9	1.71±0.03	1.67	1	1.95±0.06	1.92	-1	0.2[1]–0.32[3]
Clarithromycin	0.42±0.11	0.34	20	0.41±0.02	0.39	4	11.19±0.20	5.63	48	0.26[5]–1.2[6]
Erythromycin	0.33±0.07	0.34	-3	0.20±0.01	0.20	-4	11.28±2.10	6.13	43	0.31[1]–1.0[7]
Roxithromycin	0.00	0.00	/	0.86±0.13	1.05	-24	11.10±0.30	3.92	64	<0.1[8]–0.5[6]
Citalopram	0.47±0.08	0.46	1	0.67±0.08	0.61	8	2.52±0.15	2.06	16	0.54[2]
Venlafaxine	0.00	0.00	/	0.12±0.05	0.09	25	0.14±0.06	0.12	16	<0.1[2]

[1] (Radjenović et al., 2009) for atenolol the lowest value was in MBR sludge; [2] (Hörsing et al., 2011) for atenolol in activated sludge; [3] (Maurer et al., 2007); [4] (Sathyamoorthy et al., 2013); [5] (Göbel et al., 2005); [6] (Abegglen et al., 2009) in MBR; [7] (Xue et al., 2010) in conventional activated sludge and MBR sludge; [8] (Fernandez-Fontaina et al., 2012).
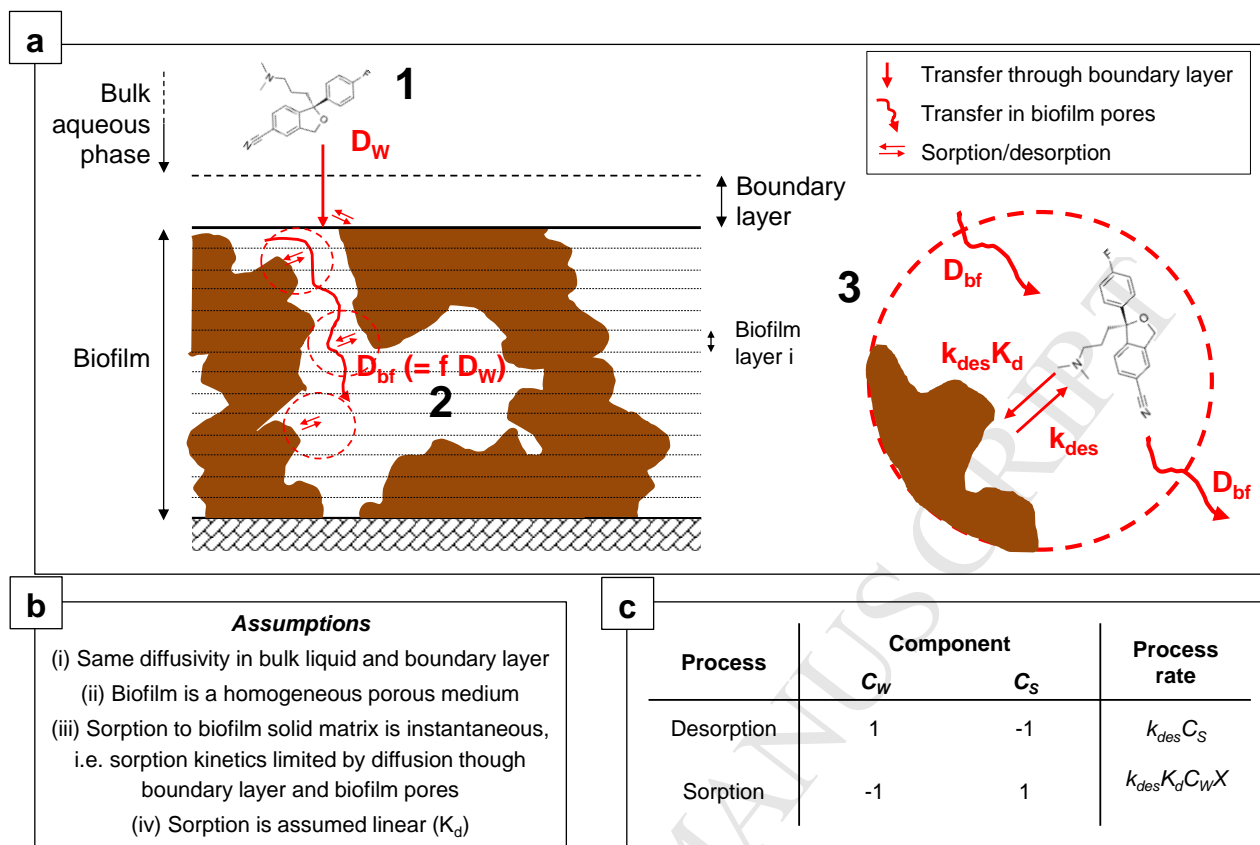
Figure 1. Conceptual model for diffusion and sorption of micropollutants into biofilms, including (a) a graphical description of the biofilm as porous medium, with discretization in 20 finite completely mixed layers, and of the consecutive steps required for partitioning onto biofilm solids (processes 1–3, see text); (b) the assumptions considered in the model; and (c) the process matrix describing sorption and desorption kinetics.
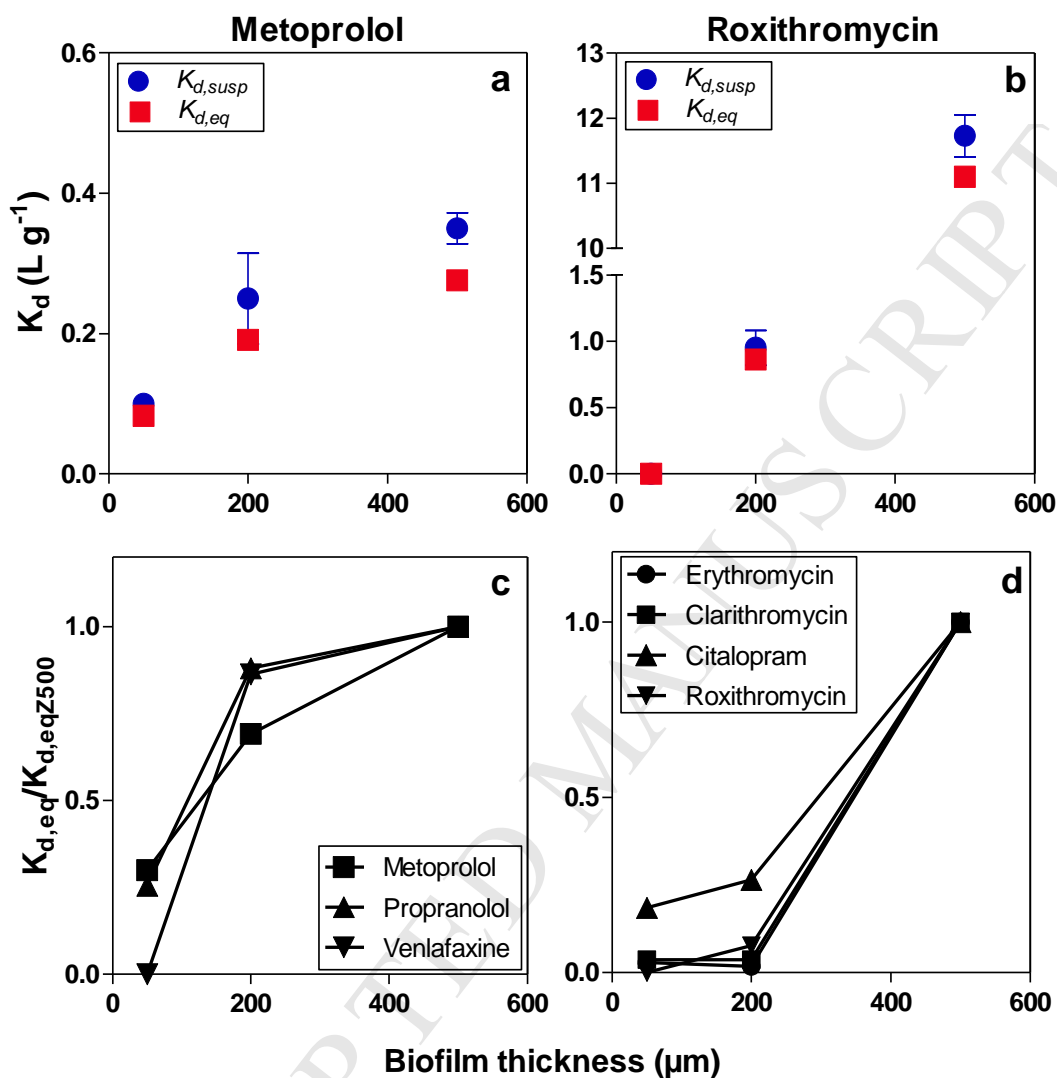
1

Figure 2. Values of the sorption coefficient calculated by accounting for and by neglecting biofilm porosity, $K_{d,susp}$ and $K_{d,eq}$, respectively for metoprolol (a) and roxithromycin (b). Different profiles of $K_{d,eq}$ normalized to $K_{d,eq,Z500}$ (i.e., for biofilm Z500) as a function of biofilm thickness are also shown for the sorptive micropollutants (c and d).
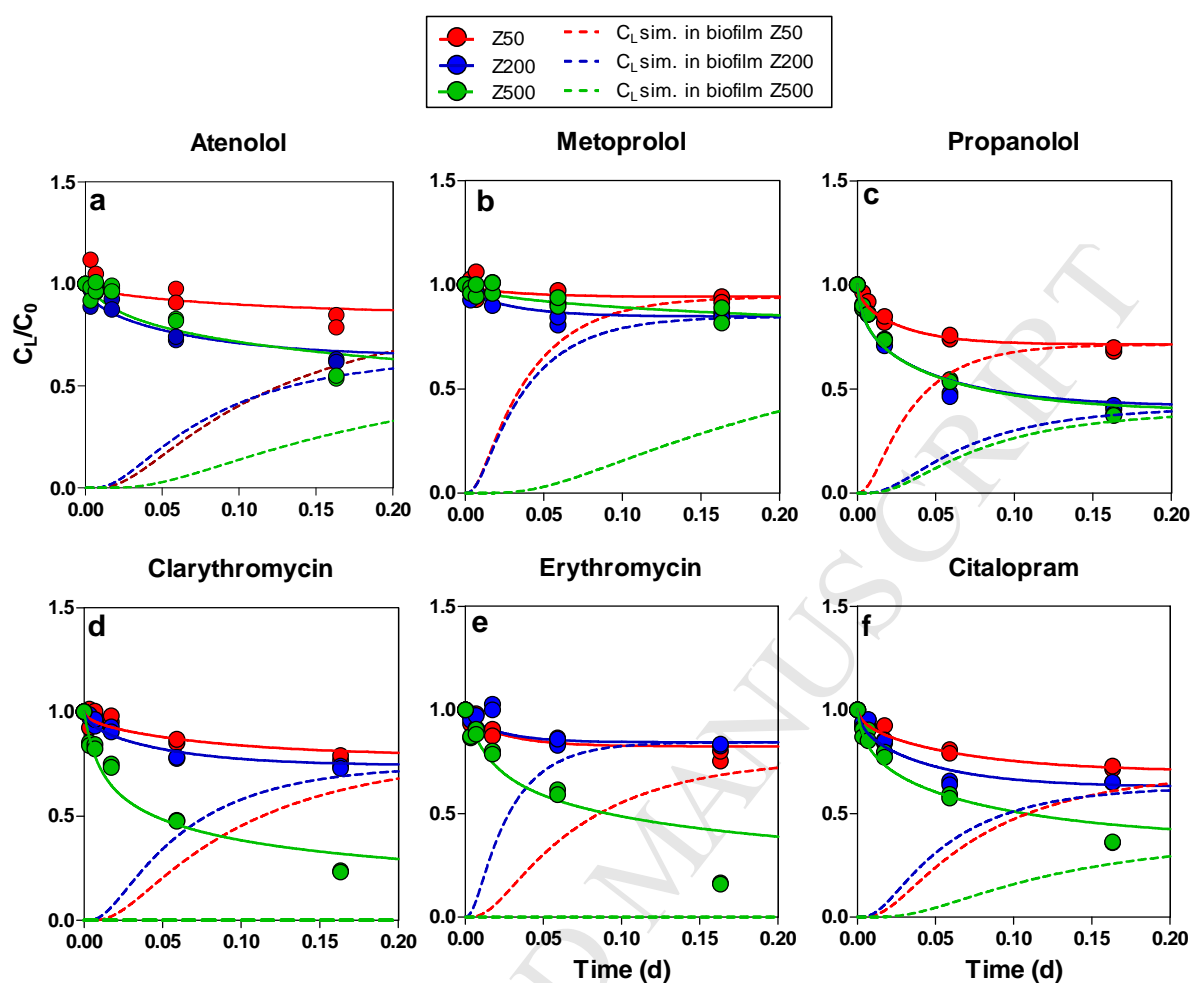
Figure 3. Measured (technical replicates, in circles) and simulated (continuous line) aqueous concentrations C_L in bulk aqueous phase (normalized over initial aqueous concentration $C_{L,0}$) and simulated concentrations in biofilm pores liquid (dashed lines) of six selected chemicals compounds during batch experiments with Z50 (red), Z200 (blue) and Z500 (green) biofilms. Simulated C_L in biofilm denotes the aqueous concentration in the deepest layer of the discretized biofilm (section 2.1).
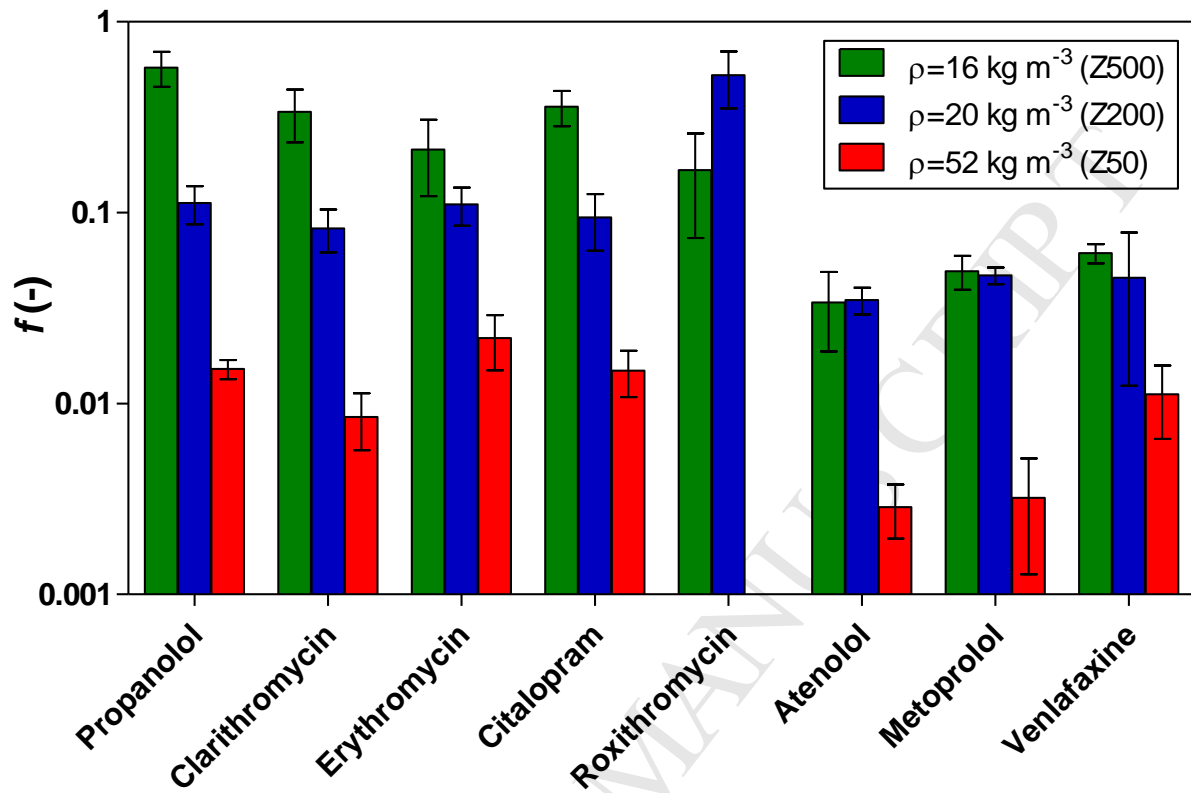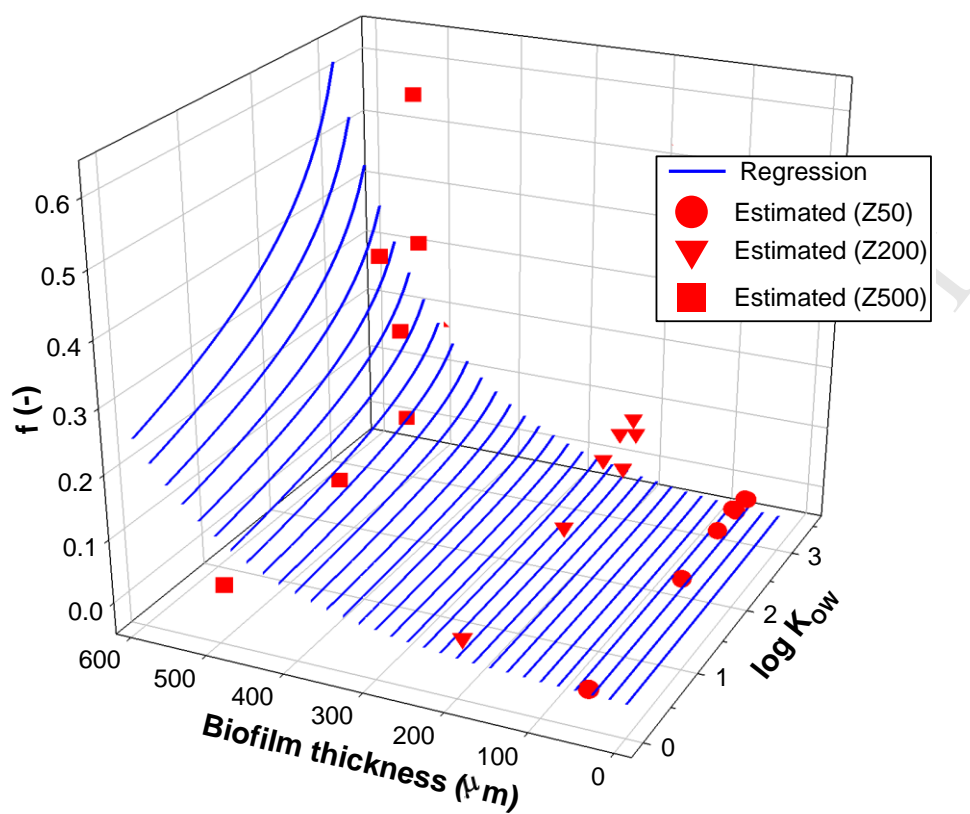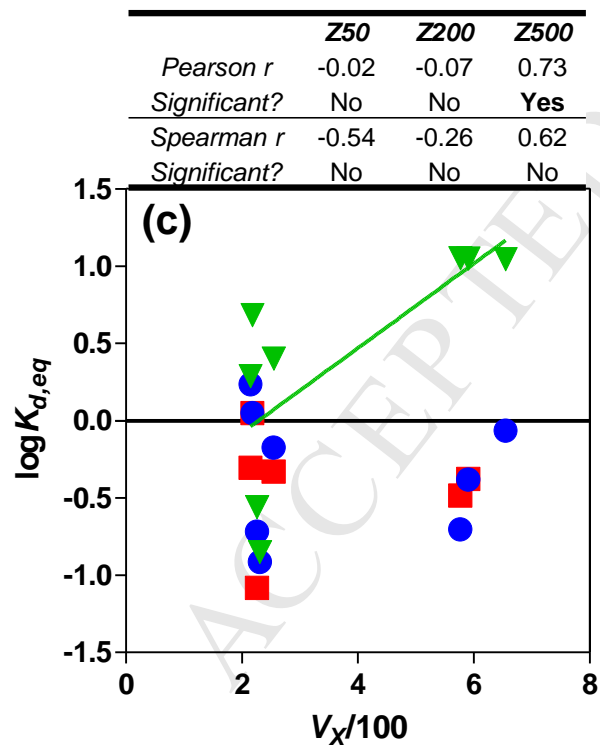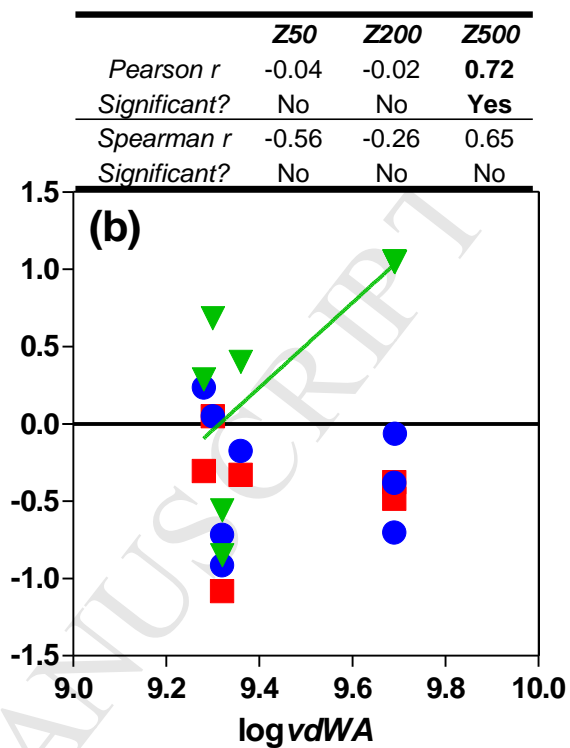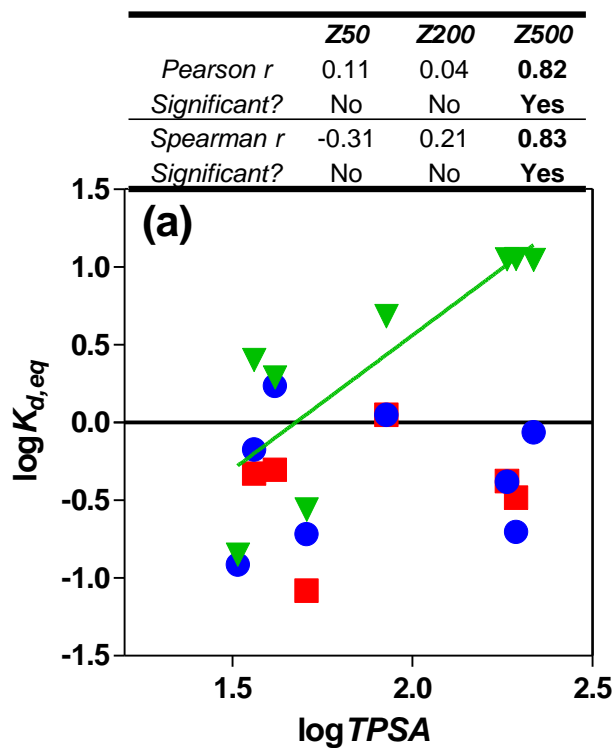
3

Figure 4. Estimated values of dimensionless effective diffusivity f for the three biofilm thicknesses and the eight chemicals – showing significant sorption – by calibrating the diffusion-sorption model.
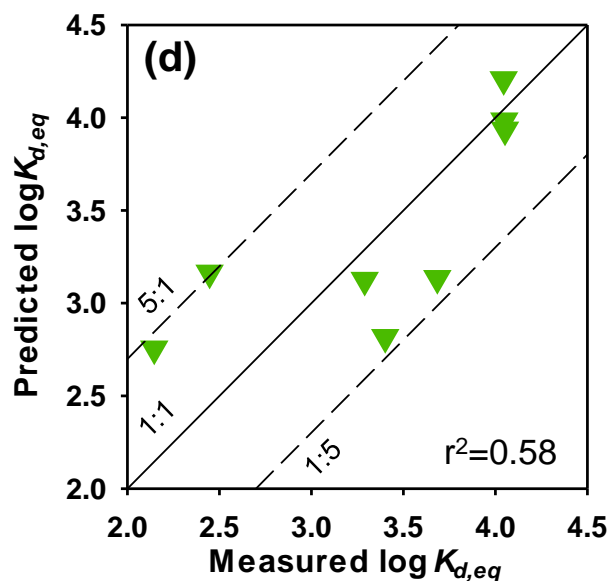
1

Figure 5. Plots of the empirical equation describing f – for atenolol, erythromycin, metoprolol,

propranolol, clarithromycin, roxithromycin, citalopram, venlafaxine – as a function of biofilm

thickness and log K_{ow}, together with estimated f values (red symbols) in Z50, Z200 and Z500.

5

(a)

	Z50	Z200	Z500
Pearson r	0.11	0.04	**0.82**
Significant?	No	No	**Yes**
Spearman r	-0.31	0.21	**0.83**
Significant?	No	No	**Yes**

(b)

	Z50	Z200	Z500
Pearson r	-0.04	-0.02	**0.72**
Significant?	No	No	**Yes**
Spearman r	-0.56	-0.26	0.65
Significant?	No	No	No

(c)

	Z50	Z200	Z500
Pearson r	-0.02	-0.07	0.73
Significant?	No	No	**Yes**
Spearman r	-0.54	-0.26	0.62
Significant?	No	No	No

$$\log K_d = 0.35 \cdot V_X/100 + 0.45 \cdot NA_i + 1.48$$

(K_d in L kg^{-1})

(d) $r^2 = 0.58$

Axis labels: $\log K_{d,eq}$, $\log TPSA$, $\log vdWA$, $V_X/100$, Predicted $\log K_{d,eq}$, Measured $\log K_{d,eq}$

Legend: Z50, Z200, Z500

Figure 6. Correlation analysis between $\log K_{d,eq}$ of the targeted micropollutants for the three biofilms (Z50, Z200, Z500) and physico-chemical descriptors: (a) $\log TPSA$; (b) $\log vdWA$; (c) McGowan's volume V_X (divided by a factor of 100). Linear regression lines were reported only for significant correlations. Based on the correlation with $V_X/100$, an empirical regression (Eq. 8) was tested according to Droge and Goss (2013a,c). The comparison between measurements and predictions using Eq. 8 (in both cases, with $K_{d,eq}$ in L kg^{-1}) is presented in (d).

Highlights

- Diffusion-sorption of pharmaceuticals assessed in biofilms of different thicknesses

- Sorption significant only for eight positively ionized compounds

- Sorption coefficients increased with increasing biofilm thickness

- Several days necessary to reach partitioning equilibrium in thicker biofilms

- Effective diffusivity in biofilm negatively influenced by biofilm density

Supplementary Information for:

Diffusion and sorption of organic micropollutants in biofilms with varying thicknesses

Elena Torresi[1,2†**], Fabio Polesel[1†], Kai Bester[3], Magnus Christensson[2], Barth F. Smets[1], Stefan Trapp[1], Henrik R. Andersen[1], Benedek Gy. Plósz[1,4]*

[1]DTU Environment, Technical University of Denmark, Bygningstorvet B115, 2800 Kongens Lyngby, Denmark

[2]Veolia Water Technologies AB, AnoxKaldnes, Klosterängsvägen 11A, SE-226 47 Lund, Sweden

[3]Department of Environmental Science, Århus University, Frederiksborgvej 399, 4000 Roskilde, Denmark

[4]Department of Chemical Engineering, University of Bath, Claverton Down, Bath BA2 7AY, UK

† The authors equally contributed to this manuscript.

*Benedek Gy. Plósz: b.g.plosz@bath.ac.uk

**Elena Torresi: elto@env.dtu.dk

Supplementary Tables

Table S1. Diffusivity coefficients in water (D_W) of the substances exhibiting sorption, estimated according to different methods from literature (see equations below).

	$D_{W,i}$ (m² d⁻¹)					
	Hayduk and Laudie (1974)	**Wilke and Chang (1955)**	**Schwarzenbach et al. (2003)**		**Trapp and Matthies (1998)**	**Sitaraman et al. (1963)**
			I	**II**		
Atenolol	$4.57 \cdot 10^{-5}$	$4.82 \cdot 10^{-5}$	$4.39 \cdot 10^{-5}$	$4.10 \cdot 10^{-5}$	$7.63 \cdot 10^{-5}$	$2.72 \cdot 10^{-5}$
Erythromycin	$2.62 \cdot 10^{-5}$	$2.74 \cdot 10^{-5}$	$2.52 \cdot 10^{-5}$	$2.10 \cdot 10^{-5}$	$4.59 \cdot 10^{-5}$	$1.75 \cdot 10^{-5}$
Metoprolol	$4.33 \cdot 10^{-5}$	$4.57 \cdot 10^{-5}$	$4.16 \cdot 10^{-5}$	$3.85 \cdot 10^{-5}$	$7.61 \cdot 10^{-5}$	$2.61 \cdot 10^{-5}$
Propranolol	$4.56 \cdot 10^{-5}$	$4.81 \cdot 10^{-5}$	$4.38 \cdot 10^{-5}$	$4.09 \cdot 10^{-5}$	$7.73 \cdot 10^{-5}$	$2.72 \cdot 10^{-5}$
Clarithromycin	$2.56 \cdot 10^{-5}$	$2.67 \cdot 10^{-5}$	$2.46 \cdot 10^{-5}$	$2.04 \cdot 10^{-5}$	$4.55 \cdot 10^{-5}$	$1.72 \cdot 10^{-5}$
Citalopram	$4.20 \cdot 10^{-5}$	$4.43 \cdot 10^{-5}$	$4.04 \cdot 10^{-5}$	$3.71 \cdot 10^{-5}$	$6.91 \cdot 10^{-5}$	$2.55 \cdot 10^{-5}$
Venlafaxine	$4.31 \cdot 10^{-5}$	$4.54 \cdot 10^{-5}$	$4.13 \cdot 10^{-5}$	$3.82 \cdot 10^{-5}$	$7.47 \cdot 10^{-5}$	$2.59 \cdot 10^{-5}$
Roxithromycin	$2.48 \cdot 10^{-5}$	$2.59 \cdot 10^{-5}$	$2.38 \cdot 10^{-5}$	$1.97 \cdot 10^{-5}$	$4.30 \cdot 10^{-5}$	$1.68 \cdot 10^{-5}$

Equations

Hayduk and Laudie (1974): $\quad D_{W,MP} = 13.26 \cdot 10^{-5} / \left(\eta^{1.14} MV_{MP}^{0.589} \right)$

Wilke and Chang (1955): $\quad D_{W,MP} = 7.4 \cdot 10^{-8} x MW^{0.5} T / \left(\eta MV_{MP}^{0.6} \right)$

Schwarzenbach et al. (2003) – I: $\quad D_{W,MP} = D_{W,ref} \left(MV_{ref} / MV_{MP} \right)^{0.589}$
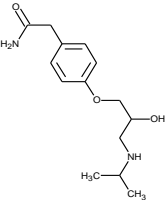
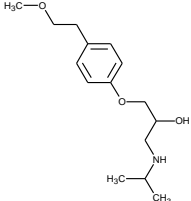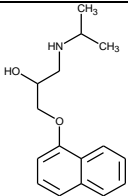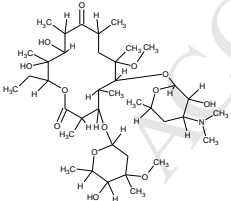Schwarzenbach et al. (2003) – II: $\quad D_{W,MP} = 2.3 \cdot 10^{-4} / MV_{MP}^{0.71}$

Trapp and Matthies (1998): $\quad D_{W,MP} = D_{W,ref} \left(MW_{ref} / MW_{MP} \right)^{0.5}$

Sitaraman et al. (1963): $\quad D_{W,MP} = 5.4 \cdot 10^{-8} MW^{0.5} T L_S^{1/3} / \left(\eta L_S^{0.3} MV_{MP}^{0.6} \right)$

where $D_{W,MP}$ = diffusivity of micropollutant ($= D_{W,i}$), η = viscosity of solvent/solution, MV_{MP} = molecular volume of the micropollutant, MW_{MP} = molecular weight of the micropollutant, T = temperature, $D_{W,ref}$ = diffusivity coefficient of reference substance, MV_{ref} = molecular volume of the reference substance, MW_{ref} = molecular weight of the reference substance, L_S = latent heat of vaporization of solvent at boiling point. Where required, oxygen was considered as reference substance ($D_{W,O2} = 2.2 \cdot 10^{-4}$ m² d⁻¹; Torresi et al., 2016). For measurement units of the different parameters, the reader is referred to the original publications.

Table S2. Physico-chemical properties of the micropollutants investigated in this study and for which sorption to MBBR biofilms was observed. Properties were estimated with ACD/Labs except for V_X (calculated according to Abraham and McGowan, 1987).

Compound	Formula	Structure	McGowan's V_X ($cm^3 mol^{-1}$)	Molecular volume MV ($cm^3 mol^{-1}$)	Molecular weight MW ($g\ mol^{-1}$)	$logK_{OW}$	$logD$	pK_a	Ref
Atenolol	$C_{14}H_{22}N_2O_3$		217.6	236.6	266.34	0.1	-1.87	9.5 (base)	ACD
Metoprolol	$C_{15}H_{25}NO_3$		226.0	258.7	267.36	1.79	0.08	9.5 (base)	ACD
Propranolol	$C_{16}H_{21}NO_2$		214.8	237.1	259.34	3.1	0.96	9.5 (base)	ACD
Clarithromycin	$C_{38}H_{69}NO_{13}$		591.4	631.9	747.9	3.16	2.12	8.5 (base)	ACD

3
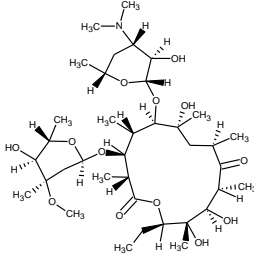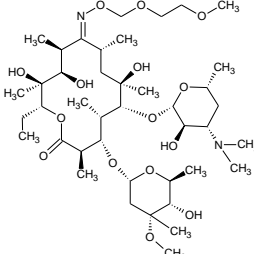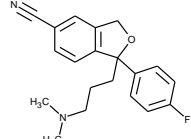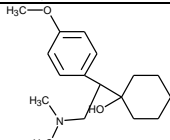
Erythromycin	$C_{37}H_{67}NO_{13}$		577.3	607.1	733.9	2.83	1.42	8.6 (base)	ACD
Roxithromycin	$C_{41}H_{76}N_2O_{15}$		655.4	666.3	837.05	3.73	2.24	8.6 (base)	ACD
Citalopram	$C_{20}H_{21}FN_2O$		255.3	272.6	324.39	2.51	2.06	9.4 (base)	ACD
Venlafaxine	$C_{17}H_{27}NO_2$		237.5	261.6	277.4	2.91	2.59	8.4 (base)	ACD

4

Table S3. Ionization properties and prevailing ionization state at experimental pH (=7.5) of all the micropollutants investigated in this study. Reported pK_a values are the ones relevant to typical wastewater pH. The chemicals, for which sorption to biofilms was observed, are presented in italics.

Compound	pK_a	Charge and ionic fraction at pH=7.5	Reference
Acetyl-sulfadiazine	6.99 (acid) 2.01 (base)	76% negative, 0% positive	ChemAxon
Sulfadiazine	6.5 (acid) 2.1 (base)	91% negative, 0% positive	ACD
Sulfamethizole	5.3 (acid) 1.8 (base)	99% negative, 0% positive	ACD
Sulfamethoxazole	5.7 (acid) 1.8 (base)	98% negative, 0% positive	ACD
Trimethoprim	7.0 (base)	24% positive	ACD
Atenolol	9.5 (base)	99% positive	ACD
Metoprolol	9.5 (base)	99% positive	ACD
Propranolol	9.5 (base)	99% positive	ACD
Sotalol	8.3 (base) 10.1 (acid)	86% positive 13% zwitterionic	ACD
Clarithromycin	8.5 (base)	92% positive	ACD
Erythromycin	8.6 (base)	92% positive	ACD
Roxithromycin	8.6 (base)	92% positive	ACD
Diclofenac	4.0 (acid)	100% negative	ACD
Phenazone	1.8 (base)	0% positive	ACD
Carbamazepine	Neutral		ACD
Citalopram	9.4 (base)	99% positive	ACD
Venlafaxine	8.4 (base)	90% positive	ACD
Diatrizoic acid	1.4 (acid)	100% negative	ACD
Iohexol	11.8 (acid)	0% negative	ACD
Iomeprol	11.8 (acid)	0% negative	ACD
Iopamidol	10.8 (acid)	0% negative	ACD
Iopromide	10.6 (acid)	0% negative	ACD

Table S4. Comparison between $K_{d,susp}$ (Eq. 6) and $K_{d,eq}$ (Eq. 3), calculated using the estimated asymptotic equilibrium concentration $C_{L,eq}$. The relative deviation Δ (%) between $K_{d,susp}$ and $K_{d,eq}$ is used to assess the impact of porosity on sorption coefficient estimation, i.e. the overestimation of the sorption coefficient by neglecting transport of micropollutants from bulk aqueous phase to biofilm pores.

	Z50			*Z200*			*Z500*		
	$K_{d,susp}$ (L g^{-1})	$K_{d,eq}$ (L g^{-1})	Δ (%)	$K_{d,susp}$ (L g^{-1})	$K_{d,eq}$ (L g^{-1})	Δ (%)	$K_{d,susp}$ (L g^{-1})	$K_{d,eq}$ (L g^{-1})	Δ (%)
Atenolol	1.15	1.12	3	1.21	1.12	8	5.15	4.84	6
Metoprolol	0.10	0.08	16	0.25	0.19	22	0.35	0.28	21
Propranolol	0.52	0.50	4	1.83	1.71	6	2.11	1.95	8
Clarithromycin	0.44	0.42	5	0.48	0.41	13	11.82	11.19	5
Erythromycin	0.35	0.33	6	0.25	0.20	22	11.91	11.28	5
Roxithromycin	0.00	0.00	/	0.95	0.86	9	11.73	11.10	5
Citalopram	0.49	0.47	5	0.74	0.67	10	2.71	2.52	7
Venlafaxine	0.03	0.00	100	0.17	0.12	30	0.21	0.14	33

Table S5. Goodness of fit (R^2) for the sorption-diffusion biofilm model, calculated by comparing measured and simulated data

	R^2		
	Z50	**Z200**	**Z500**
Atenolol	0.85	0.94	0.85
Metoprolol	0.96	0.83	0.93
Propranolol	0.99	0.97	0.98
Clarithromycin	0.93	0.97	0.94
Erythromycin	0.95	0.99	0.88
Citalopram	0.99	0.94	0.97
Venlafaxine	/	0.89	0.98
Roxithromycin	/	0.94	0.88

Table S6. Proposed models for biofilm diffusivities used in estimates validation

Diffusion model	Relation	Additional info	Range
Zhang and Bishop (1994)	$f = \varepsilon^3$	$\varepsilon = 1 - \dfrac{X_b}{\rho_{CELL}}$	$58\% < \varepsilon < 92\%$
Hinson and Kocher (1996)	$f = \dfrac{2 \cdot (1 - \varepsilon_o) \cdot \varepsilon_w}{(2 + \varepsilon_o) \cdot \left(\varepsilon_w + \dfrac{\varepsilon_p}{D_{pr}} \right)}$	$X_b = \varepsilon_o \cdot \rho_o + \varepsilon_p \cdot \rho_p$	
Beyenal et al. (1997)	$f = 10^{-0.0072367 X_b}$		
Horn and Morgenroth (2006)	$f = 1.112 - 0.019 \cdot X_b$		$10 < X_b < 20$

Where f is the dimensionless diffusivity within biofilms, X_b (kg m^{-3}) is the biofilm density, ε is the biofilm porosity, ρ_{CELL} is the cells density (250 kg·m^{-3} (Zhang and Bishop, 1994a)), ε_o is cells volume fraction, ρ_o is the cells density, ε_p is the extra polymeric substances (EPS) volume fraction, ρ_p is the EPS density (considered equal to ρ_o (Hinson and Kocher, 1996)), ε_w is the water volume fraction, and D_{pr} is the relative diffusivity within EPS (0.022 (Hinson and Kocher, 1996).
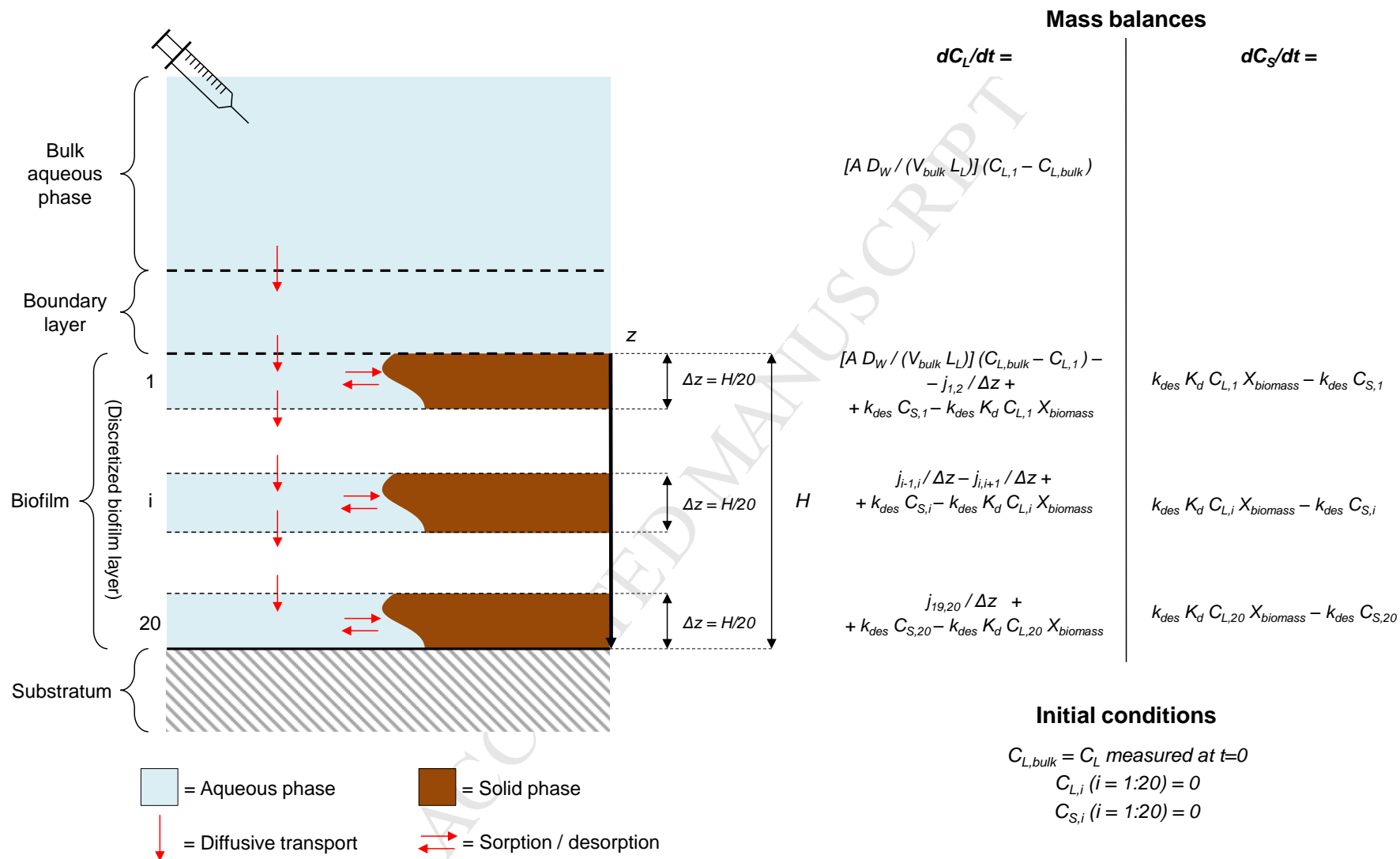
Supplementary Figures

Figure S1. Conceptual representation of the biofilm model implemented in Aquasim, with mass balances for bulk aqueous phase and selected biofilm layers and initial conditions for the state variables C_L and C_S in the different compartments.
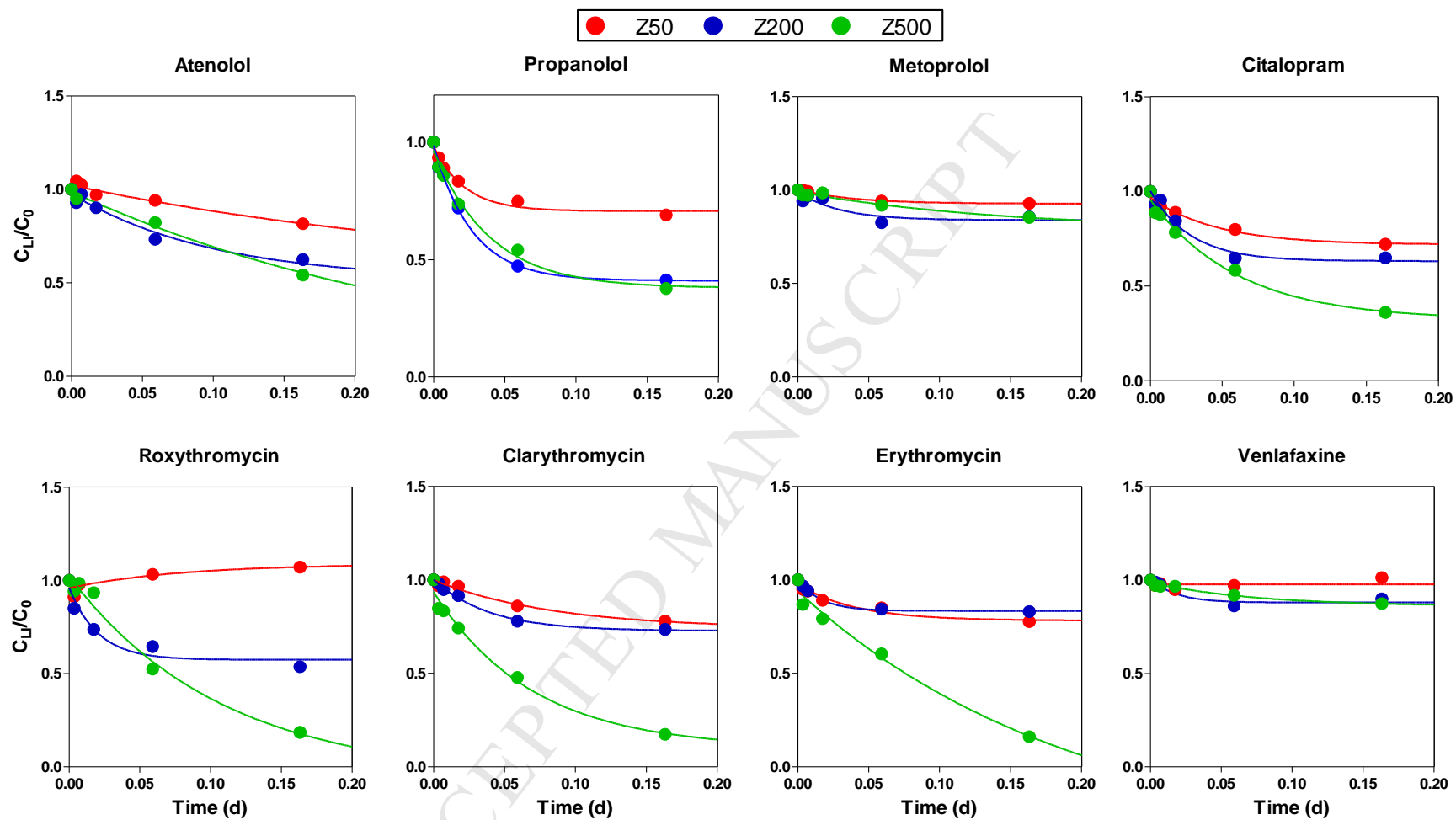
9

Figure S2. Model fit (continuous lines) of experimental data (circles) using first-order kinetics asymptotic function (Eq. 4) for the calculation of $K_{d,eq.}$
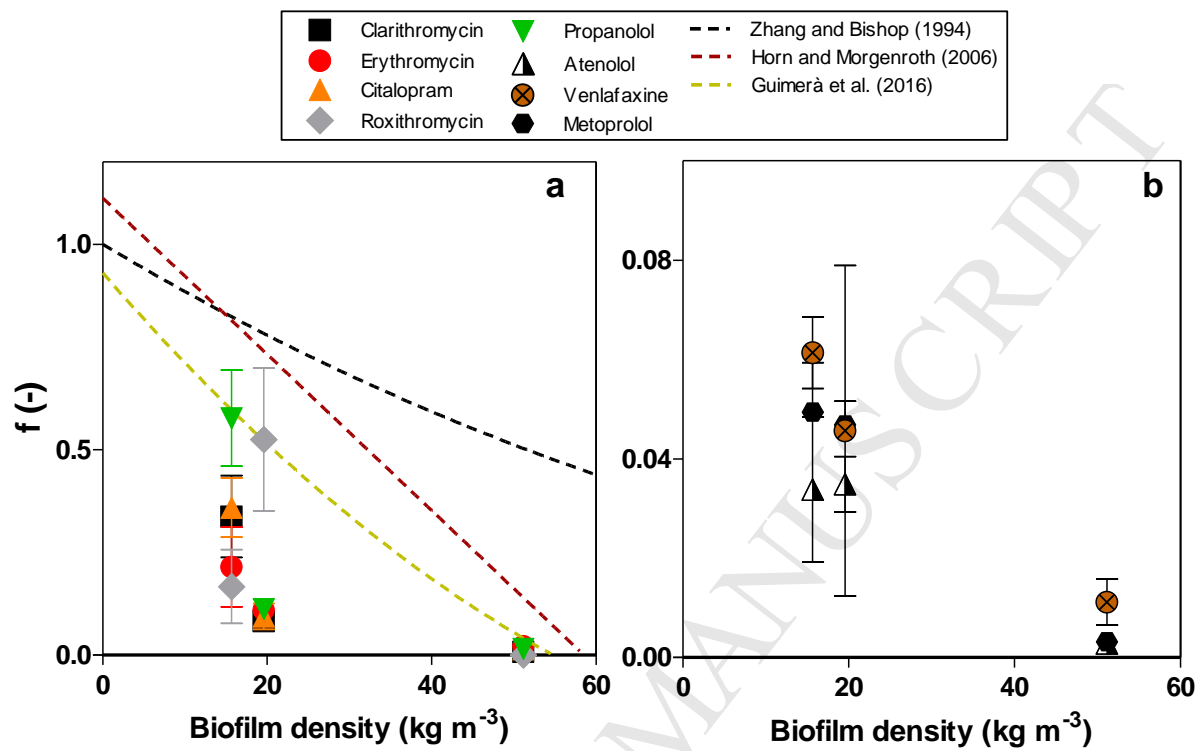
Figure S3. Estimated values of effective diffusivity cofficient *f* for the targeted micropollutants and regression correlation between f and biofilm density reported in literature.
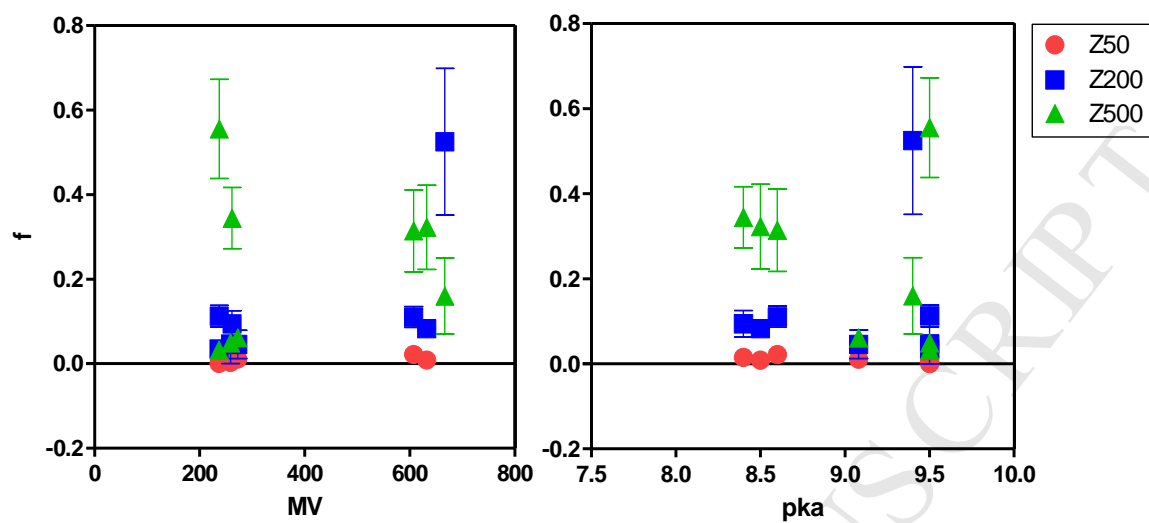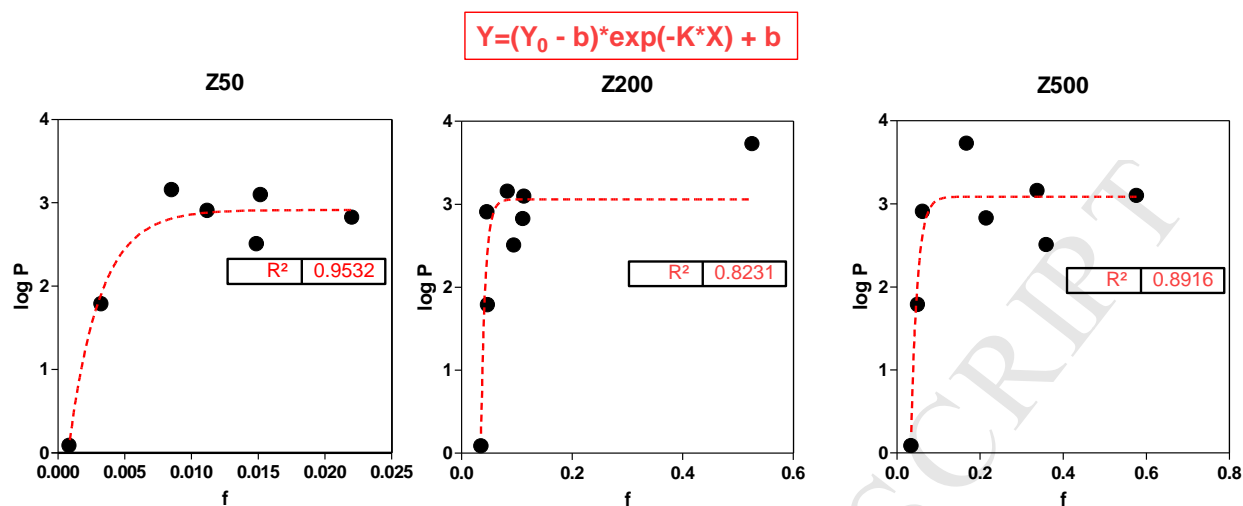
Figure S4. Estimated effective diffusivity factor (*f*) plotted as a function of molecular volume (*MV*) and dissociation constant (*pKa*) of the compounds, exhibiting sorption to biofilm.

$$Y=(Y_0 - b)*exp(-K*X) + b$$

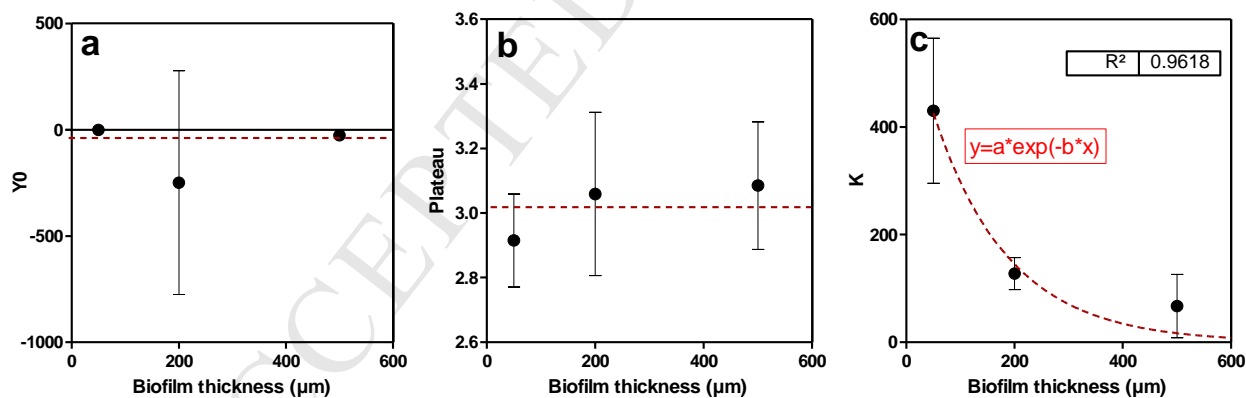|	Y0	SE Y0	b	SE b	K	SE K
Z50	-1.13	0.67	2.92	0.14	430.40	134.60
Z200	-249.40	526.10	3.06	0.25	127.50	29.79
Z500	-26.56	18.49	3.09	0.20	67.43	58.93

Figure S5. Summary of the regression, describing the diffusivity reduction factor *f* as a function of logK_{OW} (log*P*) of the chemical and biofilm thickness. Error bars indicate standard errors of the estimated regression coefficients.

	Z50	Z200	Z500
Pearson r	-0.05	-0.10	**0.72**
Significant?	No	No	**Yes**
Spearman r	-0.60	-0.24	0.57
Significant?	No	No	No

	Z50	Z200	Z500
Pearson r	0.00	0.64	-0.06
Significant?	No	No	No
Spearman r	0.33	0.59	-0.22
Significant?	No	No	No

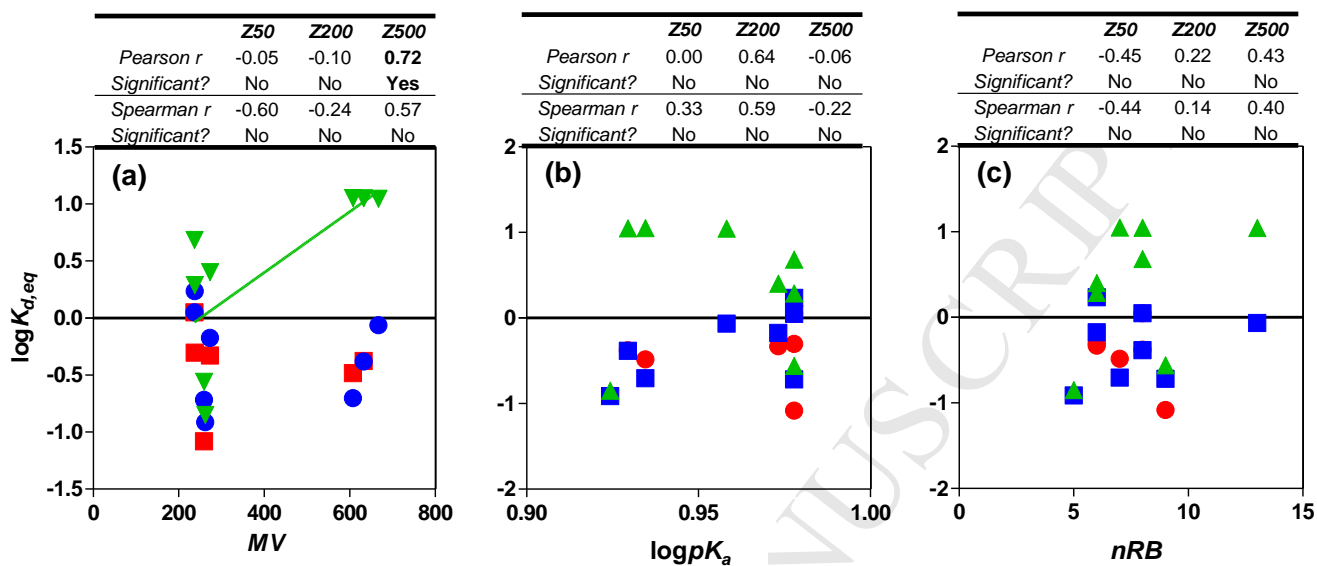|	Z50	Z200	Z500
Pearson r	-0.45	0.22	0.43
Significant?	No	No	No
Spearman r	-0.44	0.14	0.40
Significant?	No	No	No

Figure S6. Partitioning coefficients ($\log K_{d,eq}$) plotted as a function of the molecular volume (*MV*), basic dissociation constants ($\log pK_a$) and the number of rotable bonds (*nRB*).
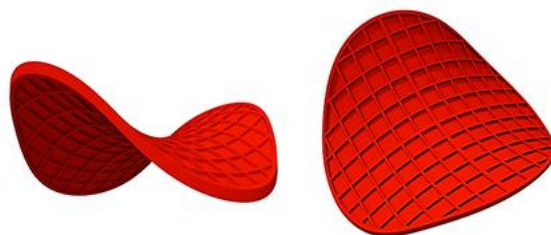

Figure S7. Drawing of Z-carriers used in this study.

Supplementary Sections

S1. Biofilm model description

The model implemented in Aquasim and used in this study is a one-dimensional biofilm model including (i) bulk aqueous phase, (ii) unstirred boundary layer and (iii) biofilm of defined maximum thickness (*H*), growing on an impermeable solid substratum of surface area *A*. The biofilm compartment consists of pore water and solid biomass, where the fraction of these two phases over the total wet biofilm volume is defined by the porosity ε and by 1-ε, respectively. One-dimensional spatial resolution of the biofilm results in concentrations and density (hence porosity) gradients along one direction only, i.e. over the biofilm depth. The following assumptions were made as to the physical structure of the biofilm, namely (i) the biofilm is at its maximum thickness *H* during sorption experiments, which is equal to the 50, 200 or 500 μm depending on the type of Z-carrier; and (ii) the biofilm has constant porosity over its depth, determining constant effective diffusivity of the pharmaceutical in the biofilm. During sorption experiments (from spiking of pharmaceuticals in bulk phase until sorption equilibrium), dynamic conditions are established in the biofilm. Overall, these conditions/assumptions define a one-dimensional dynamic biofilm model. Considering diffusive transport and reaction (sorption/desorption) processes as predominant in the biofilm, the generic microscopic mass balance in the biofilm compartment for the dissolved chemical C_L is defined by the following equation (Wanner et al., 2006):

$$\frac{\partial C_L}{\partial t} = D_{bf} \frac{\partial^2 C_L}{\partial z^2} + r \tag{Eq. S1}$$

where the term *r* denotes the rates of reaction processes. The specific form of this equation, where reaction processes included sorption to and desorption from biofilm, had already been included in the manuscript (Eq. 2).

As to the bulk aqueous phase, a mass balance can also be established considering that (i) no reaction occurs; and (ii) transfer of spiked pharmaceuticals from bulk aqueous phase to biofilms occurs via diffusive transport through the unstirred boundary layer. Under the assumptions of constant bulk aqueous phase volume (V_{bulk}) and no reaction occurring in bulk phase, the mass balance for the dissolved concentration is defined as (Wanner et al., 2006):

15

$$V_{bulk} \frac{dC_L}{dt} = \frac{AD_W}{L_L}(C_{L,bf} - C_{L,bulk})$$

(Eq. S2)

where $C_{L,bulk}$ and $C_{L,bf}$ are the dissolved concentrations in bulk phase and at biofilm surface, respectively, A is the bulk-biofilm exchange area and (equivalent to the area covered by biofilm), D_W the diffusivity in free water and L_L the boundary layer thickness. Given that $C_{L,bf} < C_{L,bulk}$ at t=0, an outward flux of dissolved pharmaceutical from bulk phase to the biofilm is established.

In this form, the model is a combination of ordinary and partial differential equations. The latter can be solved using the method lines, with discretization of the biofilm compartment into n layers (in this study $n=20$), each having the same thickness $\Delta z = H / n$. Layer 1 denotes the top biofilm, while layer 20 denotes the deepest part of the biofilm. This allows for a numerical approximation of the spatial derivate, thus for a simplification of the mathematical model from one-dimensional (with one set of partial differential equations) to zero-dimensional (with n sets of ordinary differential equations, one set for each layer). The mass balance is established in each layer for the two state variables C_L and C_S, where the latter is assumed to undergo negligible diffusive transport within the solid matrix (i.e., cannot be transported upwards or downwards in the biofilm). As described above, the mass balance for C_L included sorption, desorption and downward diffusion in each of the biofilm layers, not only in the deepest layer. Given the conditions established in the experiment and its short duration, advective transport of solubles and biofilm detachment were neglected.

The microscopic mass balance in a generic layer (i) for the dissolved mass of pharmaceuticals, considering predominant downward diffusive transport, is written as:

$dm_{L,i} / dt = $ *Diffusive mass transfer from layer (i-1) (or bulk phase) – Diffusive mass transfer to layer (i+1) + Desorption from solids in layer i – Sorption to solids in Layer i*

Diffusive mass transfer from the upper adjacent layer and to the adjacent lower layer (occurring only in pore water phase) defines the connection between different layers of the biofilm, and the "driving force" is given by the difference in dissolved concentration between adjacent layers. Mass balances in different compartments and layers, relevant to the experiments presented in this study, are given below:

16

- Bulk aqueous phase

$$\mathbf{C_L:}\ \frac{dC_{L,bulk}}{dt} = \frac{AD_W}{L_L V_{bulk}}(C_{L,1} - C_{L,bulk}) \qquad \text{(Eq. S3)}$$

$\mathbf{C_S:}$ no sorbed pharmaceuticals are present in bulk phase in the absence of suspended solids

- Layer 1 (top biofilm) – C_L and C_S in layer 1 are denoted with the subscript '1'

$$\mathbf{C_L:}\ \frac{dC_{L,1}}{dt} = \frac{AD_W}{L_L V_{bulk}}(C_{L,bulk} - C_{L,1}) - \frac{j_{1,2}}{\Delta z} - k_{des}K_d C_{L,1}X + k_{des}C_{S,1} \qquad \text{(Eq. S4)}$$

$$\mathbf{C_S:}\ \frac{dC_{S,1}}{dt} = k_{des}K_d C_{L,1}X - k_{des}C_{S,1} \qquad \text{(Eq. S5)}$$

- Layer i (inner biofilm) – C_L and C_S in layer i are denoted with the subscript 'i'. Layers $(i-1)$ and $(i+1)$ denote the layer above and below layer i.

$$\mathbf{C_L:}\ \frac{dC_{L,1}}{dt} = \frac{j_{i-1,i}}{\Delta z} - \frac{j_{i,i+1}}{\Delta z} - k_{des}K_d C_{L,i}X + k_{des}C_{S,i} \qquad \text{(Eq. S6)}$$

$$\mathbf{C_S:}\ \frac{dC_{S,i}}{dt} = k_{des}K_d C_{L,i}X - k_{des}C_{S,i} \qquad \text{(Eq. S7)}$$

- Layer 20 (deep biofilm) – C_L and C_S in layer 20 are denoted with the subscript '20'

$$\mathbf{C_L:}\ \frac{dC_{L,20}}{dt} = \frac{j_{19,20}}{\Delta z} - k_{des}K_d C_{L,20}X + k_{des}C_{S,20} \qquad \text{(Eq. S8)}$$

$$\mathbf{C_S:}\ \frac{dC_{S,20}}{dt} = k_{des}K_d C_{L,20}X - k_{des}C_{S,20} \qquad \text{(Eq. S9)}$$

The generic term $j\ /\ \Delta z$ (g m^{-3} d^{-1}) describes the diffusive mass transfer between adjacent layers as a simplification of the second order derivative $D_{bf}\ \partial^2 C\ /\ \Delta z^2$. The two subscripts of the mass flux j (g m^{-2} d^{-1}) indicate the layer from which and to diffusive mass transfer occurs, respectively. Based on Fick's first law of diffusion ($j = -D\ \partial C/\partial z$), the flux j is a function of the effective diffusivity D_{bf} and of the concentration gradient between adjacent layers, i.e. the driving force for diffusive transport. Further

17

details on the numerical methods used to approximate partial differential equations to ordinary differential equations through spatial discretization can be found in Reichert (1994).

Initial conditions for C_L and C_S in different compartments were established based on measurements and assumptions, i.e.:

Bulk aqueous phase

$C_L = C_L$ measured at t=0

$C_S = 0$ (no solids were assumed to be present in the bulk aqueous phase, since the effluent was pre-filtered – see Lines 225–226)

Biofilm (both pore water and solids in each layer *i*)

$C_{L,i} = 0$ (the pore water at t=0 did not contain any mass of pharmaceuticals, since spiking occurred in the bulk aqueous phase)

$C_{S,i} = 0$ (the biofilm was pre-washed with tap water overnight to allow for desorption of previously sorbed pharmaceuticals – see also Lines 223–224)

A schematic representation of the system and of the biofilm discretization, as well as of the mass balances in the system and initial conditions for the state variables, is shown in Figure S1.

S2. Biofilm properties

Biomass dry density in biofilm (ρ_d, g cm^{-3}) was calculated based on Eq. S10 (Tchobanoglous and Burton 1991; Hu et al., 2013):

$$\frac{M_s}{\rho_d} = \frac{M_f}{\rho_f} + \frac{M_v}{\rho_v} \qquad \text{(Eq. S10)}$$

where M_s (g) is the dry mass of biofilm solids (expressed as total attached solids, TAS), M_f (g) the dry mass of fixed mineral solids in the biofilm (expressed as total fixed solids, TFS), ρ_f the density of fixed solids (=2.5 gTFS cm^{-3}), M_v (g) the dry mass of volatile solids in the biofilm (expressed as total volatile solids, TVS), and ρ_v the density of volatile solids (=1 gTVS cm^{-3}).

The biofilm volume not occupied by pores, i.e. including water inside the cells but excluding water outside the cells, was calculated as (Eq. S11):

$$V_W = \frac{\dfrac{M_s}{\rho_d}}{1 - W_{wi}}$$ (Eq. S11)

where W_{wi} is the water content inside the cells (=80% of total cell biomass) (Hu et al., 2013; Zhang and Bishop, 1994b). Thus, biofilm porosity (%) was calculated as (Eq. S12):

$$\varepsilon = 1 - \frac{V_W}{V_{bf}}$$ (Eq. S12)

where V_{bf} (m^3) is the total biofilm volume (volume of wet biofilm including pore water volume, determined from nominal surface area and biofilm thickness of each Z-carrier type). The pore water volume V_{PW} (m^3) was eventually determined as (Eq. S13):

$$V_{PW} = \varepsilon \cdot V_{bf} = V_{bf} - V_W$$ (Eq. S13)

Finally, the biofilm density (gTAS m^{-3}) was calculated as (Eq. S14):

$$\rho = \frac{M_s}{V_{bf}}$$ (Eq. S14)

We note that biofilm density ρ (Eq. S14) denotes the mass of (microbial) biomass per volume of wet biofilm (i.e., defines a concentration within the biofilm), while the dry biofilm density ρ_d denotes the weight of dry biofilm per volume of dry biofilm (i.e., defines a *true* density).

The thickness of the boundary layer, L_L (μm), was assumed to be equal to 10 μm for all the Z-carriers. L_L can be estimated, based on fluid dynamics principles, as a function of the characteristic length of the carrier L_C (the flow-through radius of the biofilm carrier minus the biofilm thickness) and the non-dimensional Sherwood number (Boltz et al., 2011). When considering Z-carriers design, L_C is minimized as most of the interstitial space is occupied by the biofilm (Torresi et al., 2016). Thus, L_L was selected by considering the lowest value reported in literature (Brockmann et al., 2008; Joss et al., 2004). It is likely that the high flow rate of nitrogen sparging during batch experiments may have further minimized L_L, as previously considered (Wicke et al., 2007). Furthermore, comparable L_L values have been used for fate modelling of illicit drugs (having similar $D_{W,i}$ with the chemicals assessed in this study) in sewer biofilms (Ramin et al., submitted).

S3. Derivation of the adjusted partition coefficient (Equation 5)

Based on mass conservation principles, the mass of pharmaceuticals spiked at t=0 in the bulk phase is equivalent to the total mass at the end of sorption experiments. Hence, the following mass balance can be written (in the absence of any biological or abiotic degradation of pharmaceuticals):

Mass spiked in bulk phase (t=0) = Remaining mass in bulk phase + Mass dissolved in pore water +
+ Mass sorbed to biofilm solids

The above mass balance can be translated in the following equation:

$$C_{L,0}V_{bulk} = C_{L,eq}V_{bulk} + C_{L,eq}V_{PW} + C_{S,eq}^{*}M_{X,biomass} \tag{Eq. S15}$$

where $C_{L,0}$ and $C_{L,eq}$ [µg L^{-1}] are the dissolved pharmaceuticals concentrations at t=0 and at equilibrium, respectively; $C_{S,eq}$* [µg g^{-1}] is the sorbed concentration and the superscript '*' is used to distinguish it from $C_{S,eq}$ [µg L^{-1}] as defined in the main text; V_{bulk} and V_{PW} [L] are the volumes of bulk aqueous phase and pore water, respectively; and $M_{X,biomass}$ [g] is the mass of solids in the system.

The mass of solids can be defined as the product of the concentration of solids in the system and the total volume of the system:

$$M_{X,biomass} = X_{biomass}(V_{bulk} + V_{bf,wet}) \tag{Eq. S16}$$

where $X_{biomass}$ [g L^{-1}] denotes the concentration of solids as defined in the manuscript text (0.8 g L^{-1}) and $V_{bf,wet}$ [L] is the volume of wet biofilm (= surface area of Z carriers · biofilm thickness, also equal to the sum of pore water volume and volume occupied by solids in biofilm).

Hence, the last term of the sum can be rearranged as:

$$C_{S,eq}^{*}M_{X,biomass} = C_{S,eq}^{*}X_{biomass}(V_{bulk} + V_{bf,wet}) = C_{S,eq}(V_{bulk} + V_{bf,wet}) \tag{Eq. S17}$$

where $C_{S,eq}$ [µg L^{-1}] is the sorbed concentration of pharmaceuticals as defined in the main text (e.g., Eqs. 3 and 4).

By rearranging the mass balance, we can write:

$$C_{S,eq}(V_{bulk} + V_{bf,wet}) = C_{L,0}V_{bulk} - C_{L,eq}V_{bulk} - C_{L,eq}V_{PW} \tag{Eq. S18}$$

and it follows that:

$$C_{S,eq} = C_{L,0}V_{bulk}/(V_{bulk} + V_{bf,wet}) - C_{L,eq}(V_{bulk} + V_{PW})/(V_{bulk} + V_{bf,wet}) \tag{Eq. S19}$$

Eventually, the adjusted partition coefficient K_d (accounting for the pharmaceutical concentration dissolved in pore water) can be written as:

$$K_d = C_{S,eq}/(C_{L,eq}X_{biomass}) = \left[C_{L,0}V_{bulk}/(V_{bulk}+V_{bf,wet}) - C_{L,eq}(V_{bulk}+V_{PW})/(V_{bulk}+V_{bf,wet})\right]/(C_{L,eq}X_{biomass})$$

$$\text{(Eq. S20)}$$

which is also presented as Equation 5 in the main manuscript text.

S4. Proposed empirical correlation for effective diffusivity coefficient f

An exponential equation was first used to correlate f with $\log K_{OW}$ at each biofilm thickness (Fig. S3). Secondly, the intercept (y_0), the asymptotic coefficient b (corresponding to the maximum log K_{OW}) and the slope (k) (see Fig. S4) estimated separately for Z50, Z200 and Z500 were plotted against biofilm thickness (Fig. S4, a–c). While no trend was observed for y_0 and b with biofilm thickness, a second exponential equation was used to correlate values of slope (k) of the three biofilms with biofilm thickness. The obtained relationship is presented in Eq. S21

$$f = \frac{1}{488 \cdot e^{-0.0072L_F}} \ln\left(\frac{-12.7 - \log K_{ow,max}}{\log K_{ow} - \log K_{ow,max}}\right)$$

$$\text{(Eq. S21)}$$

where L_F is the biofilm thickness (μm) and $\log K_{ow,max}$ is the asymptotic $\log K_{ow}$ which approximate the one reported for the targeted compounds in this study.

21

References

Beyenal, H., Seker, S., Tanyolaç, A., 1997. Diffusion Coefficients of Phenol and Oxygen in a Biofilm of Pseudomonas putida. AIChE J. 43, 243–250.

Boltz, J.P., Morgenroth, E., Brockmann, D., Bott, C., Gellner, W.J., Vanrolleghem, P.A., 2011. Systematic evaluation of biofilm models for engineering practice: components and critical assumptions. Water Sci. Technol. 64, 930.

Brockmann, D., Rosenwinkel, K.H., Morgenroth, E., 2008. Practical identifiability of biokinetic parameters of a model describing two-step nitrification in biofilms. Biotechnol. Bioeng. 101, 497–514.

Hayduk, W., Laudie, H., 1974. Prediction of diffusion coefficients for nonelectrolytes in dilute aqueous solutions. AIChE J. 20, 611–615.

Hinson, R.K., Kocher, W.M., 1996. Model for effective diffusivities in aerobic biofilms 122, 1023–1030.

Horn, H., Morgenroth, E., 2006. Transport of oxygen, sodium chloride, and sodium nitrate in biofilms. Chem. Eng. Sci. 61, 1347–1356.

Hu, M., Zhang, T.C., Stansbury, J., Neal, J., Garboczi, E.J., 2013. Determination of Porosity and Thickness of Biofilm Attached on Irregular-Shaped Media. J. Environ. Eng. 139, 923–931.

Joss, A., Andersen, H., Ternes, T., Richle, P.R., Siegrist, H., 2004. Removal of estrogens in municipal wastewater treatment under aerobic and anaerobic conditions: consequences for plant optimization. Appendix: Diffusive mass transfer across the boundary layer and inside the floc. Environ. Sci. Technol. 38, 3047–55.

Piculell, M., Welander, P., Jönsson, K., Welander, T., 2016. Evaluating the Effect of Biofilm Thickness on Nitrification in Moving Bed Biofilm Reactors 37, 732–743.

Ramin, P., Libonati Brock, A., Causanilles, A., Valverde-Pérez, B., Emke, E., de Voogt, P., Polesel, F., Plósz, B.G. Transformation and sorption of illicit drug biomarkers in sewer biofilms. Submitted to

Environ. Sci. Technol.

Reichert, P., 1994b. Concepts underlying a computer program for the identification and simulation of aquatic systems. Swiss Federal Institute for Environmental Science and Technology (EAWAG), Dübendorf, Switzerland.

Schwarzenbach, R.P., Gschwend, P.M., Imboden, D.M., 2003. Environmental Organic Chemistry (2nd edition). John Wiley & Sons, Inc., Hoboken, NJ, US.

Sitaraman, R., Ibrahim, S.H., Kuloor, N.R., 1963. A generalized equation for diffusion of liquids. J. Chem. Eng. Data 8, 198–201.

Tchobanoglous G., Burton F., Stensel H., Wastewater Engineering Treatment and Reuse, 4th ed., Metcalf and Eddy, Inc., McGraw-Hill Company, New York, 2003.

Torresi, E., Fowler, J.S., Polesel, F., Bester, K., Andersen, H.R., Smets, B.F., Plosz, B.G., Christensson, M., 2016. Biofilm thickness influences biodiversity in nitrifying MBBRs – Implications on micropollutant removal. Environ. Sci. Technol. 50, 9279–9288.

Trapp, S., Matthies, M., 1998. Transport and Transformation of Compounds in Soil, in: Chemodynamics and Environmental Modeling. Springer-Verlag.

Wanner, O., Eberl, H.J., Morgenroth, E., Noguera, D.R., Picioreanu, C., Rittmann, B.E., van Loosdrecht, M.C.M., 2006. Mathematical modeling of biofilms. IWA Publishing.

Wicke, D., Bockelmann, U., Reemtsma, T., 2007. Experimental and modeling approach to study sorption of dissolved hydrophobic organic contaminants to microbial biofilms. Water Res. 41, 2202–2210.

Wilke, C.R., Chang, P., 1955. Correlation of diffusion coefficients in dilute solutions. AIChe J. 1, 264–270.

Zhang, T.C., Bishop, P.L., 1994a. Evaluation of tortuosity factors and effective diffusivities in biofilms. Water Res. 28, 2279–2287.

Zhang, T.C., Bishop, P.L., 1994b. Density, porosity, and pore structure of biofilms. Water Res. 28,

24

2267–2277.